## **FULL PAPER**





# Structural and energetic properties of RMX<sub>3</sub>-NH<sub>3</sub> complexes

James A. Phillips<sup>1</sup> | Anna R. Ley<sup>1</sup> | Patrick W. Treacy<sup>1</sup> | Benjamin M. Wahl<sup>1</sup> | Brittany C. Zehner<sup>1</sup> | Kelling J. Donald<sup>2</sup> | Samuel Gillespie<sup>2</sup>

#### Correspondence

James A. Phillips, Department of Chemistry and Biochemistry, University of Wisconsin -Eau Claire, 105 Garfield Ave, Eau Claire, WI 54701.

Email: phillija@uwec.edu

Kelling J. Donald, Department of Chemistry, Gottwald Center for the Sciences, University of Richmond, 28 Westhampton Way, Richmond, VA 23173. Email: kdonald@richmond.edu

## Funding information

National Science Foundation, Grant/Award Numbers: 0958696, 1056430, 1229354, 1566035, 1626238

## **Abstract**

We have explored the structural and energetic properties of a series of RMX<sub>3</sub>-NH<sub>3</sub> (M=Si, Ge; X=F, Cl; R=CH<sub>3</sub>, C<sub>6</sub>H<sub>5</sub>) complexes using density functional theory and low-temperature infrared spectroscopy. In the minimum-energy structures, the NH<sub>3</sub> binds axially to the metal, opposite a halogen, while the organic group resides in an equatorial site. Remarkably, the primary mode of interaction in several of these systems seems to be hydrogen bonding (C-H--N) rather than a tetrel (N $\rightarrow$ M) interaction. This is particularly clear for the RMCl<sub>3</sub>-NH<sub>3</sub> complexes, and analyses of the charge distributions of the acid fragment corroborate this assessment. We also identified a set of metastable geometries in which the ammonia binds opposite the organic substituent in an axial orientation. Acid fragment charge analyses also provide a clear rationale as to why these configurations are less stable than the minimum-energy structures. Matrix-isolation infrared spectra provide clear evidence for the occurrence of the minimum-energy form of CH<sub>3</sub>SiCl<sub>3</sub>-NH<sub>3</sub>, but analogous results for CH<sub>3</sub>GeCl<sub>3</sub>-NH<sub>3</sub> are less conclusive. Computational scans of the M-N distance potentials for CH<sub>3</sub>SiCl<sub>3</sub>-NH<sub>3</sub> and CH<sub>3</sub>GeCl<sub>3</sub>-NH<sub>3</sub>, both in the gas phase and bulk dielectric media, reveal a great deal of anharmonicity and a propensity for condensed-phase structural change.

#### KEYWORDS

hydrogen bonding, molecular complexes, molecular machines, sigma holes, tetrel bonding

# 1 | INTRODUCTION

Interest in the structure and bonding of molecular complexes (also called "charge-transfer" or "donor-acceptor" complexes) has persisted for many decades. Most notably perhaps, Odd Hassel centered the lecture celebrating his 1969 Nobel prize on "Structural Aspects of Interatomic Charge-Transfer Bonding."<sup>[1]</sup> A substantial review,<sup>[2]</sup> as well as several monographs,<sup>[3-6]</sup> was published around that time as well, and in those initial works, the foundational ideas regarding the bonding interactions in these systems were outlined. More recently, interest has been spurred, at least in part, by quantum-chemical investigations of molecular complexes,<sup>[7,8]</sup> which have revealed, more clearly, the underlying nature of the interactions in these systems. In addition, these studies have led to the onset of newly named subcategories, including "halogen" bonding,<sup>[9,10]</sup> as well as "triel"<sup>[11]</sup> and "tetrel" bonding,<sup>[12]</sup> for which the names acknowledge the geometries about the coordination centers, which in turn affect the symmetry properties of the electron-deficient regions and acceptor orbitals. In all of these cases, however, the fundamental acid-base bonding motif (electron-donor to electron-acceptor) prevails.

This article was published online on 8 August 2020. An error was subsequently identified in the group name in the first page footnote. This notice is included in the online version to indicate that it has been corrected on 13 August 2020.

The collaboration that manifested this manuscript stemmed directly from interactions between students from the respective institutions at the annual MERCURY Conference. This meeting is an intimate, student-centred conference, in which undergraduates have the opportunity to interact directly with one another and discuss their research. In this instance, a student from the Donald Group initially noticed a peculiar result on a poster presented by Phillips Group students, and when they followed up on these results, a dialogue between the PI's ensued, ultimately rendering this manuscript.

<sup>&</sup>lt;sup>1</sup>Department of Chemistry and Biochemistry, University of Wisconsin - Eau Claire, Eau Claire, Wisconsin

<sup>&</sup>lt;sup>2</sup>Department of Chemistry, Gottwald Center for the Sciences, University of Richmond, Richmond, Virginia

One particularly comprehensive theoretical investigation of donor-acceptor systems appeared in the literature at about the time when the use of models incorporating electron correlation was becoming widespread, [7] and others followed in the years since. [8,13] One notable outcome of these studies was the observation of a broad range of interactions, reflected in both strength and structure, spanning from long, weak, van der Waals-type contacts to much shorter and stronger cases, in-line with bona fide dative bonds. Moreover, one inescapable conclusion was that there was no fixed proportion of the electrostatic, charge-transfer, or dispersion contributions to the overall bonding in such complexes. Rather, the influence of each contribution is very sensitive to the type of complex and the specific pairs involved, and no single factor seems to correlate with strength in any overarching manner. [7,8,13]

Another reason for the continued interest in these systems over the last two decades is a tendency for some complexes to undergo large changes in structure between the gas phase and various condensed-phase media. The underlying principle is that any stabilizing medium—such as a solvent, the solid-state, or even a noble gas matrix—may cause the donor-acceptor bond to contract relative to the gas phase, and there is a corollary distortion of the Lewis acid unit. For example, in the case of HCN-BF3, the measured gas-phase B-N distance is 2.47 Å, but the bond shortens in the crystalline solid to a value of 1.65 Å, while the N-B-F angle opens by almost  $14^{\circ}$ . Similarly, for FCH2CN-BF3, the predicted (B3PW91/aug-cc-pVTZ) structure has a B-N distance of 2.42 Å, but the value in the crystal structure is 1.64 Å.

In the Phillips group, we have been primarily concerned with the extent to which bulk media affect molecular complexes in this regard, and of particular interest are the effects of inert noble gas matrices: solid argon, nitrogen, and neon. [15,19] Much of our initial work focused on nitrile-BF3 systems, which are classified as  $\pi$ -hole complexes, [20] due to the nature of the electron-deficient region in the BF3 acceptor. In addition, due to the three-coordinate acceptor moiety, the interactions in these systems are referred to as "triel" bonds. [11] For FCH2CN-BF3, we observed a systematic red shift for the B-F asymmetric stretching frequency across various media: gas phase (BPW91/aug-cc-pVTZ) < Ne (s) < Ar(s) < N2 (s). [21] These shifts spanned a range of about 250 cm<sup>-1</sup>, and they were systematic, paralleling the charge-stabilizing ability of the medium (eg. polarizability, dielectric constant, etc.), in a manner that was consistent with a progressive contraction of the B-N bond across these environments. Furthermore, computational scans of the interaction energy over a range of B-N distances revealed significant energetic changes that take place in bulk media along this reaction coordinate and ultimately provided mechanistic insight into the experimentally observed bond contractions. [15,21,22] In general, the complexes prone to substantial structural changes in the condensed phase exhibit a notably flat donor-acceptor potential, with a global minimum at a long, essentially nonbonded distance, and only a gradual energy rise toward the inner wall, perhaps only a few kcal/mol over several tenths of an angstrom. Because the complexes are more polar at short distances, usually due to increased charge transfer and a greater degree of geometrical distortion in the acceptor unit, the solvation energy increases preferentially in the inner regions of the potential, and the minimum shifts to shorter values—if the curve is sufficiently flat, that is, the energy range is comparable in magnitude to the energy of solvat

Subsequent studies of nitrogen-donor-MX<sub>4</sub> complexes (M=Si, Ge, Ti; X=F, Cl)<sup>[23-25]</sup> revealed some indication of condensed-phase structural changes, but overall, those were much less dramatic than the observations noted above for the B-N systems. One striking example was CH<sub>3</sub>CN-SiF<sub>4</sub>, for which a theory predicted a long gas-phase Si-N distance of about 3.0 Å that would shorten by over 1.0 Å in low-dielectric media ( $\varepsilon$ =5). However, no experimental evidence of this extraordinary structural change could be observed via low-temperature IR spectroscopy measurements.<sup>[23]</sup> More subtle effects were predicted for both nitrile-GeF<sub>4</sub><sup>[23,24]</sup> and imine-SiF<sub>4</sub> complexes,<sup>[25]</sup> but a complicating factor with these systems is that the stable reaction products that result from the direct mixing of donor and acceptor are a 2:1 complexes (eg, GeF<sub>4</sub>(NCCH<sub>3</sub>)<sub>2</sub>) with a six-coordinate metal. This obscures any direct comparisons to the solid state with regard to the analogous 1:1 system. Nonetheless, for GeF<sub>4</sub>(NCCH<sub>2</sub>F)<sub>2</sub>, a 0.2 Å difference was noted between the Ge-N distances of the (predicted) gas-phase and (measured) solid-state structures, and solid-state IR spectra are consistent with similar effects for GeF<sub>4</sub>(NCCH<sub>3</sub>)<sub>2</sub> and GeF<sub>4</sub>(NCCH<sub>2</sub>Cl)<sub>2</sub><sup>[24]</sup>

The Donald group has recently investigated a series of tetrel-type donor-acceptor complexes involving various  $MX_4^{[26]}$  and  $MXH_3^{[27]}$  acceptors and showed that the sigma-hole concept is useful in rationalizing the structure and bonding in those systems. The use of the term 'sigma-hole' has proliferated in the literature over the roughly 13 years since its debut. It describes the depletion in the charge density on atom Y outside the bonding region about the bond axis in an R-Y sigma bond, where R is an electron-withdrawing substituent. If R is sufficiently electronegative relative to Y, a positive potential may arise in that sigma-hole region on Y around the extension of the R-Y bond, which is typically described as a "positive sigma hole" or, perhaps misleadingly, as simply a 'sigma-hole'. Donald et al. posit<sup>[26]</sup> that the presence of such positive potentials promotes charge transfer into  $\sigma^*$  orbitals on the acceptor such as SiF<sub>4</sub> in F<sub>4</sub>Si $\leftarrow$ NH<sub>3</sub>; for example, the R-Y  $\sigma^*$  orbital coincides typically with the extension of the R-Y bond axis such that both the electrostatic and changed transfer interactions are oriented in the same direction. Moreover, factors that stabilize one of those two contributions to the bonding—such as substituting for a more electron-withdrawing R fragment—will strengthen both the electrostatic and change-transfer contributions to the bonding by stabilizing the acceptor LUMO and strengthening the sigma-hole. That is so, even if—as one article claimed quite recently electrostatic contribution to the bonding is more dominant in some forms of donor-acceptor interactions with strong sigma-holes.

In this manuscript, we will report the structural and energetic properties of the ammonia complexes of a series of  $RMX_3$  acceptors (M=Si, Ge; X=F, Cl; R=CH<sub>3</sub>, C<sub>6</sub>H<sub>5</sub>), which are the monomethyl and monophenyl analogs of the  $MX_4$  acids that we have studied previously. These systems are effective probes of the sigma-hole model because they have distinctly different regions of positive potentials lying opposite the M-X and M-C bonds. These complexes are also of practical interest with regard to possible materials chemistry applications. The organic groups offer a means of linking these potentially "tunable" bonds to larger structures, wherein a response to a change in chemical environment or other stimulus would allow one to



modify the structural and electronic properties. Thus, one could possibly induce a force within a chain, molecular wire, or other larger assembly. In this work, we report equilibrium structures and binding energies and M-N potentials curves for this series of complexes, as well as analyses of the fragment charge distributions. In addition, we will present results from infrared spectra of cryogenic Ar matrices doped with  $NH_3$  and  $CH_3SiCl_3$  or  $CH_3GeCl_3$  that are generally consistent with the weak interactions predicted for equilibrium structures of  $CH_3SiCl_3-NH_3$  and, to some extent,  $CH_3GeCl_3-NH_3$  as well.

#### 2 | MATERIALS AND METHODS

## 2.1 | Computational methods

All computations were performed using Gaussian 09 version B.0.1 and D.0.1. [31] In order to find the most reliable method for predicting acid frequency shifts, which are essential for assigning and interpreting the low-temperature IR results, [15,32] we conducted a validation study based on the experimental frequencies of  $CH_3SiCl_3$  and  $CH_3SiCl_3$  and used five density functional theory methods [33] (M06, [34] B3LYP, [33]  $\omega$ B97X-D, [35] M06-2X, [34] and M05 [34]), as well as MP2, [33] with the aug-cc-pVTZ [33] basis set. The argon-matrix frequencies for  $CH_3SiCl_3$  and  $CH_3GeCl_3$  that were obtained in this study were used as a validation benchmark. For both compounds, we found that M06 produced the lowest root-mean-squared error in predicting the six experimentally observed vibrational modes for each acid fragment.

For the complexes, one set of initial structure searches was performed using a variety of methods, including M06, M06-2X,  $\omega$ B97X-D, and MP2, with a series of basis sets ranging from 6-31G(d) to cc-pVTZ. In these searches, four basic coordination geometries were first considered; they were generated by placing the organic group and base in the axial or equatorial positions about a five-coordinate M center. Equilibrium conformations were then located by rotating the organic or NH<sub>3</sub> substituent accordingly upon the observation of imaginary torsional frequencies. In parallel, another set of geometry optimizations, at the M06/aug-cc-pVTZ level, was carried out by considering each symmetric ( $C_s$ ) conformation of the four geometrical isomers (16 in total for the complexes with R=CH<sub>3</sub>). In the end, two types of stable structures were located: the "R-equatorial" forms, in which the NH<sub>3</sub> unit binds axially to the metal atom, while the organic binds equatorially, and the "R-axial" forms, in which both organic and NH<sub>3</sub> bind axially to the metal.

For the reported structures, equilibrium geometries were obtained with convergence set criteria using the "opt=tight" condition and utilized an ultra-fine integration grid. As a whole, the global minima were difficult to locate, presumably due to flat intermolecular potential surfaces, especially with regard to torsional motions, and some of the complexes exhibited several shallow minima. Often, it was essential to use force constants to guide the geometry optimizations (via the "opt=calcfc" option) in order to locate true minima, which lacked imaginary frequencies. Ultimately, several of the final equilibrium structures lacked symmetry and were identified by relaxing symmetry upon the observation of imaginary frequencies (usually for torsional motions). In addition, in a few instances, these results were double-checked using "opt=verytight". Ultimately, we chose to report the M06/aug-cc-pVTZ structures, but these were verified at the  $\omega$ B97X-D and M06-2X levels as well.

A natural bond orbital (NBO)<sup>[36]</sup> analysis was carried out (also at the M06 level) for all fragments involved in these complexes, and we obtained computed point charges obtained from the natural population analysis,<sup>[37]</sup> as well as dipole moments. Electrostatic potential maps were generated using the Gaussian View program by plotting the computed electrostatic potentials on the 0.001 au isodensity surface.

For CH<sub>3</sub>SiCl<sub>3</sub>–NH<sub>3</sub> and CH<sub>3</sub>GeCl<sub>3</sub>–NH<sub>3</sub>, N-M potential energy curves were mapped in a point-wise manner at a series of fixed distances ranging from 1.5 to 4.5 Å for H<sub>3</sub>N–SiCl<sub>3</sub>CH<sub>3</sub> and 1.8 to 4.0 Å for H<sub>3</sub>N–GeCl<sub>3</sub>CH<sub>3</sub>, in 0.1 Å increments. All degrees of freedom aside from the fixed N-M distances were optimized at each point along these curves. For H<sub>3</sub>N–SiCl<sub>3</sub>CH<sub>3</sub>, the method dependence was explored explicitly by comparing results from  $\omega$ B97X-D, M06, M06-2X, and M05, in addition to the CCSD energies of the M06 geometries (CCDS//M06), all with the aug-cc-pVTZ basis set. M06 was chosen as the primary method for subsequent investigations of the potentials because the energies agreed reasonably well with the CCSD values along the curve, and as noted above, M06 was chosen for the reported structural results. Condensed-phase effects on the N-Si and N-Ge potentials of the R-equatorial configurations of CH<sub>3</sub>SiCl<sub>3</sub>–NH<sub>3</sub> and CH<sub>3</sub>GeCl<sub>3</sub>–NH<sub>3</sub> were explored by incorporating solvation free energies from the polarized continuum model (PCM)<sup>[38]</sup> into the M06 energies (ie, PCM/M06/aug-cc-pVTZ), with dielectric constants ranging from 1.5 to 10.0 and other solvent parameters left at their default settings (ie, for water).

# 2.2 | Materials

Chemicals used in this study include trichloromethylsilane (EMD Millipore, >99%), trichloromethylgermane (Alfa Aesar, >97%), anhydrous ammonia (Praxair, >99.5%), and argon (Praxair, >99.99%). Prior to making gas mixtures for matrix-isolation experiments, SiCl<sub>3</sub>CH<sub>3</sub> and GeCl<sub>3</sub>CH<sub>3</sub> were purified via several freeze-pump-thaw cycles, but for bulk reactivity experiments, they were used without further purification. Gases were also used without further purification.

# 2.3 | Bulk-phase reactivity

Direct, bulk-phase reactions between  $NH_3$  and  $SiCl_3CH_3$  or  $GeCl_3CH_3$  were carried out by adding gaseous  $NH_3$  to a sealed Schlenk tube (with a Teflon stopcock sidearm) containing neat liquid  $SiCl_3CH_3$  or  $GeCl_3CH_3$ . First, 2 to 3 mL of liquid  $SiCl_3CH_3$  or  $GeCl_3CH_3$  was added to the tube, and it was capped with a rubber septum. Ammonia was the added via the Teflon tube fitted with a hypodermic needle, which was punctured through the septum. The stopcock was opened slightly to allow excess gas to escape prior to initiating the flow of  $NH_3$ . Solid white products formed immediately when the  $NH_3$  entered the tube, and a slight temperature increase was noted. The  $NH_3$  flow was continued until it had appeared that the reaction was completed. Both solid products were air stable and showed no obvious signs of decomposition when the tubes were stored in a cabinet for several months. The products were insoluble in most solvents, and attempts to grow crystals via solvent diffusion were largely unsuccessful, aside from one sample that turned out to be crystals of  $NH_4Cl$  (s), presumably an elimination product. At this point, these solid products remain uncharacterized, but the efforts to identify and characterize them continue.

## 2.4 | Matrix-isolation infrared spectra

Matrix-isolation IR spectra were obtained using a previously described apparatus based on a Cyromech ST-15 optical cryostat. Gas mixtures (NH $_3$  in Ar and CH $_3$ SiCl $_3$  or CH $_3$ GeCl $_3$  in Ar) were prepared in 2-L glass bulbs (Chemglass) on a preparatory glass vacuum line. This system is maintained at a pressure of about  $1 \times 10^{-4}$  Torr using a glass diffusion pump (Chemglass AF-0330). Mixture concentrations ranged from 1/1600 to 1/400 (CH $_3$ MCl $_3$ /Ar or NH $_3$ /Ar). For experiments involving both NH $_3$  and CH $_3$ SiCl $_3$  or CH $_3$ GeCl $_3$ , matrix samples were deposited by allowing the mixtures to flow through separate Teflon lines that merged immediately prior to entering the cryostat chamber by using a custom-designed, colinear mixing flange. This is essential to prevent the formation of reaction products prior to deposition. For control experiments involving only NH $_3$  or CH $_3$ SiCl $_3$  or CH $_3$ GeCl $_3$ , only one of these deposition lines was operated. In any event, the gas mixtures were ultimately condensed on a KBr window inside that cryostat vacuum chamber. Sample temperatures were controlled using a Scientific Instruments #9600 temperature controller and silicon diode located at the end of the refrigeration stage. Spectra were recorded using a Thermo Scientific Nicolet iS10 FT-IR with 1-cm $^{-1}$  resolution. Typically, 400 scans were averaged (both background and sample) to obtain the final spectra. In most cases, two 60-minute depositions were conducted at temperatures ranging from 15 to 20 K, and subsequently, most samples were annealed for 60 minutes at 30 K. Spectra were recorded between depositions and after annealing.

## 3 | RESULTS AND DISCUSSION

#### 3.1 | Fragment properties

For reference, we have displayed computed geometries (M06/aug-cc-PVTZ) for the acid fragments in Figure 1. For the most part, these overall geometries are retained in the complexes. The exceptions are  $CH_3CF_3$  and  $C_6H_5CF_3$ , for which the corresponding complexes are significantly stronger than the other six. There are, however, some slight structural distortions that take place in the weaker complexes, which do shed some light on the nature of the interactions therein. The computed geometry of  $NH_3$  has the expected  $C_{3v}$  structure with an N-H distance of 1.011 Å and an H-N-H angle of 107.0°.

As noted above, the M06 method was selected as the preferred method for the equilibrium structure results because it most accurately predicted the five measured (argon-matrix) vibrational frequencies of the commercially available acid fragments,  $CH_3SiCl_3$  and  $CH_3SiCl_3$ . Experimental and theoretical (harmonic) frequencies, with methods as indicated and the aug-cc-pVTZ basis set, are listed in Tables 1 and 2 for  $CH_3SiCl_3$  and  $CH_3GeCl_3$ , respectively; a scaling factor was not applied to the theoretical values. The root-mean-square (RMS) errors of the M06 predictions for  $CH_3SiCl_3$  and  $CH_3GeCl_3$  were 8.9 and 28.5 cm<sup>-1</sup>, respectively. The latter error is notably larger, and as a whole, the  $CH_3GeCl_3$  predictions are less accurate. This may be due, in part, to isotopic composition; the predictions are strictly for  $^{74}Ge$  isotopomer, while the measured frequencies reflect an average of five naturally occurring isotopes of germanium. It is worth noting that we have also found M06 to be optimal in two recent studies of related  $MF_4$  complexes,  $^{[24,25]}$  in which we used a similar validation procedure. In all cases, the goal is to make effective comparisons between the experimental and theoretical frequencies of the various complexes (vide infra).

## 3.2 | Equilibrium structures: Global minima

As noted above, all four possible geometrical isomers were considered in both sets of structural searches, that is, the four permutations that arise from placing the  $NH_3$  subunit and R substituent ( $CH_3$  or  $C_6H_5$ ) in the axial or equatorial locations about the five-coordinate metal. We will utilize the "axial" and "equatorial" terminology that formally pertains to a trigonal-bipyramidal geometry about the metal, in spite of the fact that the acid

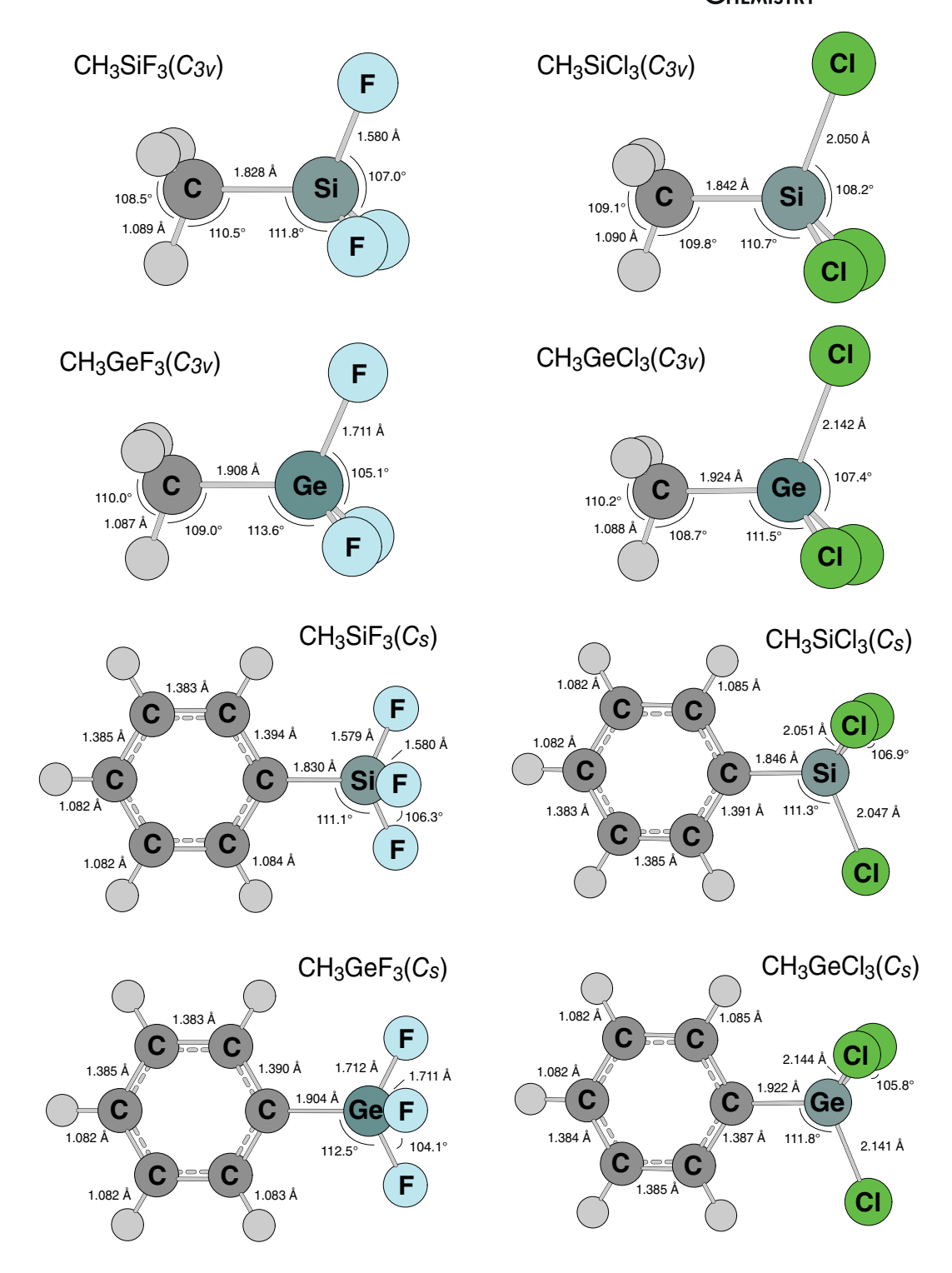


FIGURE 1 Computed M06/aug-cc-pVTZ equilibrium structures of the acid fragments, with symmetry as indicated

fragments retain their near-tetrahedral geometries in most of the complexes. The exceptions are the RGeF<sub>3</sub> systems, but even in these cases, the acid fragment is only partially distorted, and the geometries are intermediate between the tetrahedral and trigonal bipyramidal ideals. As a whole, these were difficult structure searches, and it is clear that the intermolecular potential surfaces in these systems are flat, especially with regard to angular and torsional degrees of freedom. Furthermore, additional meta-stable structures were identified in several cases.

In all cases, the two possible geometries in which the  $NH_3$  was initially placed in an equatorial site were found to be unstable; they optimized to other structural forms. For each stable complex, the minimum-energy structure had the  $NH_3$  bound in an axial manner, opposite a halogen, with the organic substituent in an equatorial position. We will refer to these configurations as "methyl-equatorial" or "phenyl-equatorial" as appropriate

| Mode\method <sup>b</sup>                      | B3LYP | ωB97X-D | M05  | M06  | M06-2X | MP2  | Exp.c |
|---|-------|---------|------|------|--------|------|-------|
| Si-Cl assy stretch <sup>d</sup>               | 558   | 580     | 579  | 573  | 582    | 590  | 575   |
| Si-C stretch                                  | 745   | 768     | 745  | 759  | 778    | 774  | 761   |
| CH <sub>3</sub> Wag                           | 829   | 827     | 813  | 800  | 816    | 823  | 799   |
| CH <sub>3</sub> "umbrella" (SB) <sup>d</sup>  | 1299  | 1304    | 1264 | 1265 | 1291   | 1294 | 1266  |
| CH <sub>3</sub> deformation (AB) <sup>d</sup> | 1454  | 1456    | 1433 | 1422 | 1450   | 1466 | 1411  |
| RMS error                                     | 33.3  | 32.8    | 15.5 | 5.8  | 26.2   | 34.4 | _     |

**TABLE 1** Measured and calculated frequencies<sup>a</sup> for CH<sub>3</sub>SiCl<sub>3</sub>

<sup>&</sup>lt;sup>d</sup>For these frequencies, there are two nearly-degenerate modes, symmetric (A') and asymmetric (A''), in the  $C_s$  point group, which are predicted to be split by 1 cm<sup>-1</sup> or less and not resolved in our measurements. "AB" and "SB" signify "Symmetric Bend" and "Asymmetric Bend", respectively.

| Mode\method <sup>b</sup>                      | B3LYP | ωB97X-D | M05  | M06  | M06-2X | MP2  | Exp.c |
|---|-------|---------|------|------|--------|------|-------|
| Ge-Cl assy stretch <sup>d</sup>               | 415   | 431     | 430  | 434  | 441    | 452  | 434   |
| Ge-C stretch                                  | 604   | 632     | 627  | 627  | 638    | 657  | 629   |
| CH <sub>3</sub> Wag                           | 835   | 833     | 821  | 803  | 815    | 803  | 821   |
| CH <sub>3</sub> "umbrella" (SB) <sup>d</sup>  | 1274  | 1287    | 1249 | 1241 | 1277   | 1272 | 1258  |
| CH <sub>3</sub> deformation (AB) <sup>d</sup> | 1455  | 1458    | 1434 | 1421 | 1454   | 1462 | 1407  |
| RMS error                                     | 61.2  | 60.0    | 28.9 | 28.6 | 52.3   | 68.2 | -     |

**TABLE 2** Measured and calculated frequencies<sup>a</sup> for CH<sub>3</sub>GeCl<sub>3</sub>

henceforth or, in general, as the "R-equatorial" geometries. The fact that these structures comprise the global minima are consistent with the sigma-hole model, which would predict that the strongest sigma-holes reside opposite the halogens (vide infra). In addition, the structures with both the NH<sub>3</sub> and the organic substituent oriented axially, opposite one another, were not only found to be stable but also several kcal/mol higher in energy than the global-minimum, R-equatorial structures. We will refer to these meta-stable geometries as "methyl-axial" or "phenyl-axial" as appropriate henceforth or, in general, as the "R-axial" structures. The quasistability of these structures is also consistent with the sigma-hole model: the ammonia resides opposite the organic group, which also manifests a sigma-hole, but it is not as strong as that opposite the halogens (vide infra). In the unstable, NH<sub>3</sub>-equatorial structures, there is no atom/group directly opposite the donor, and thus, no sigma-hole interactions occur at these locations. However, it appears that tetrel-like interactions between the NH<sub>3</sub> and the metal center are not the primary interactions in many of the minimum-energy geometries discussed below.

The minimum-energy methyl-equatorial and phenyl-equatorial structures of the  $CH_3MX_3-NH_3$  complexes are displayed in Figures 2 and 3, respectively, and the corresponding thermochemical data are listed in Table 3. Overall, the M-N distances are extremely long in all cases except for  $CH_3GeF_3-NH_3$  and  $C_6H_5GeF_3-NH_3$ . In fact, aside from these two systems, the other complexes are extremely weak, with long M-N distances ranging from 3.2 to almost 4.0 Å, near or sometimes exceeding the sums of the corresponding van der Walls radii (3.65 Å for Si-N and 3.66 Å for Ge-N). The binding energies range from 3.9 to 5.2 kcal/mol. In fact, for most of these systems, X=Cl in particular, it appears that any N-M tetrel-like interactions are missing or likely compromised; the acid geometries are nearly tetrahedral, and the  $NH_3$  subunits are tilted toward a C-H bond on the R fragment in a manner that nearly aligns the  $C_3$  axis of the ammonia with a C-H hydrogen. This seems to indicate C-H--N hydrogen bonding. In addition, in five of these six weaker systems, the exception being  $CH_3SiF_3-NH_3$ , the N-H distances are less than the sum of the N and H van der Waals radii (2.65 Å). Some additional observations pertaining to these interactions will be discussed below when the complexes are considered in detail. As for the RGeF<sub>3</sub> systems, they exhibit evidence of moderately strong  $N\rightarrow Ge$  dative bonds, with binding energies of about 9 kcal/mol and acid geometries that are significantly distorted, although the extent of this deformation is clearly intermediate. In addition, at about 2.3 Å, the Ge-N distances are a few tenths of an Angstrom longer than the sum of the Ge and N covalent radii (1.91 Å).

The weaker three of the methyl-containing complexes displayed in Figure 2 adopt the same overall structural type. For  $CH_3SiF_3-NH_3$ , the  $NH_3$  binds in a symmetrical manner, opposite one of the halogens (effectively axial), with the out-of-plane hydrogens eclipsing the equatorial

<sup>&</sup>lt;sup>a</sup>Units of cm<sup>-1</sup>.

<sup>&</sup>lt;sup>b</sup>Harmonic values from each stated method with the aug-cc-pVTZ basis set.

<sup>&</sup>lt;sup>c</sup>Experimental values obtained in argon-matrix experiments; the uncertainty is about ±1 cm<sup>-1</sup>.

aUnits of cm<sup>-1</sup>.

<sup>&</sup>lt;sup>b</sup>Harmonic values from each stated method with the aug-cc-pVTZ basis set.

<sup>&</sup>lt;sup>c</sup>Experimental values obtained in argon-matrix experiments; the uncertainty is about ±1 cm<sup>-1</sup>.

<sup>&</sup>lt;sup>d</sup>For these frequencies, there are two nearly-degenerate modes, symmetric (A') and asymmetric (A"), in the  $C_s$  point group, which are predicted to be split by 1 cm<sup>-1</sup> or less and not resolved in our measurements. "AB" and "SB" signify "Symmetric Bend" and "Asymmetric Bend", respectively.

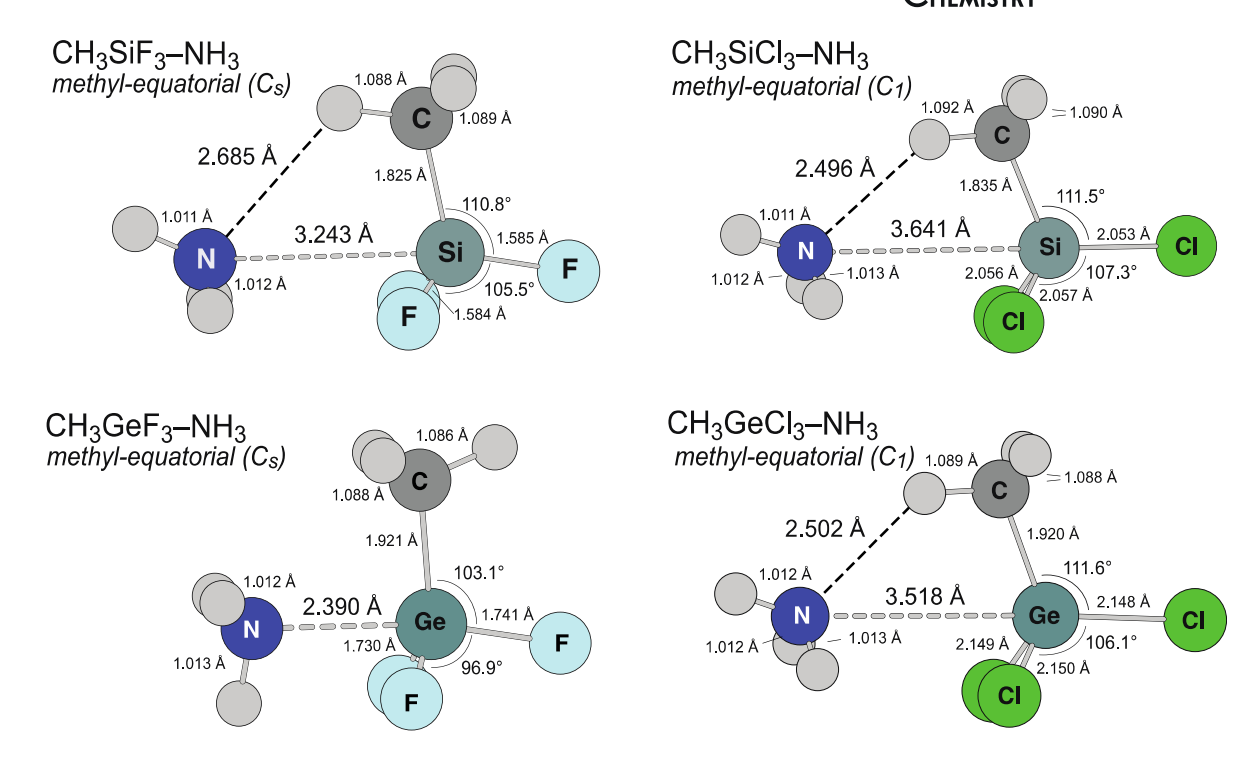


**FIGURE 2** Minimum-energy, methyl-equatorial structures  $CH_3MX_3-NH_3$  complexes via M06/aug-cc-pVTZ. The  $CH_3SiCl_3-NH_3$  and  $CH_3GeCl_3-NH_3$  complexes exhibit slight deviations from  $C_5$  symmetry; in addition to the minor bond length differences distances noted, the  $NH_3$  subunit is tilted such that the upper-left N-H bond is rotated forward, out of the plane of the page

halogens.  $CH_3SiCl_3-NH_3$  and  $CH_3GeCl_3-NH_3$  are similar, but these deviate slightly from  $C_5$  symmetry; the  $NH_3$  is rotated by 11.1 and 16.5°, relative to that in the  $CH_3SiF_3-NH_3$ . One truly noteworthy feature in all three of these geometries for the weaker methyl-containing systems is that the  $NH_3$  is tilted to direct its lone pair toward the adjacent, in-plane (for the acid fragment) hydrogen, suggestive of a weak hydrogen bonding interaction.

The N-H distances for  $CH_3SiCl_3-NH_3$  and  $CH_3GeCl_3-NH_3$  are 2.495 and 2.502 Å, respectively, which are about 0.15 Å shorter than the predicted van der Waals contact distance (2.65 Å). In addition, the in-plane C-H bonds in the  $CH_3SiCl_3$  and  $CH_3GeCl_3$  subunits are very slightly elongated, by 0.002 and 0.001 Å, respectively. For  $H_3N-SiF_3CH_3$ , the N-H distance (2.685 Å) is about 0.2 Å longer and more comparable to the sum of the N and H van der Waals radii, while the Si-N distance (3.213 Å) is about 0.4 Å shorter than the predicted van der Waals contact distance and that of  $H_3N-SiCl_3CH_3$ . There is also no appreciable elongation of the in-plane C-H bond. These observations seem to indicate that a weak N-Si tetrel interaction accompanies any hydrogen bonding, certainly more so than in  $CH_3SiCl_3-NH_3$ . It seems also possible that these weaker methyl-containing complexes are further stabilized by favorable electrostatic interactions between the  $NH_3$  hydrogens and the halogens they eclipse (or nearly) on the acid subunit. These H-X distances are about 2.8 to 3.0 Å, but if these interactions were appreciably strong, it would conflict with the observation that the  $NH_3$  is a nearly free rotor in these complexes.

In contrast,  $CH_3GeF_3-NH_3$  exhibits some key structural differences from its three weaker counterparts, beyond a fairly short Ge-F distance and a significantly distorted coordination geometry about the Ge. In this case, the  $NH_3$  is in a staggered conformation relative to the  $GeF_3$  framework, while the  $CH_3$  and  $GeF_3$  are eclipsed (the free  $CH_3GeF_3$  structure is staggered, see Figure 1). The upshot of this is that there is no C-H-N interaction, and a  $Ge \rightarrow N$  dative bond is the primary interaction. The acid geometry is only partially distorted; however, the bond angles displayed in Figure 2 (96.9° and 103.1°) lie between the values for the ideal tetrahedral and trigonal bipyramidal geometries. This suggests a tetrel bond of intermediate strength, consistent with the binding energy value relative to other systems, a Ge-N distance that is fairly short yet still about 0.3 Å longer than the sum of the covalent radii.

The detailed aspects of the structures of the phenyl complexes (Figure 3) largely parallel the structures of their methyl counterparts, but there are some key differences. Again, for the three relatively weak systems,  $C_6H_5SiF_3-NH_3$ ,  $C_6H_5SiCl_3-NH_3$ , and  $C_6H_5GeCl_3-NH_3$ , the out-of-plane  $NH_3$  hydrogens are approximately eclipsed with the corresponding halogens. Specifically,  $C_6H_5SiF_3-NH_3$  is symmetric, and the hydrogens are essentially eclipsing the halogens. However, similar to  $CH_3SiCl_3-NH_3$  and  $CH_3GeCl_3-NH_3$  above, the  $NH_3$  subunits in  $C_6H_5SiCl_3-NH_3$  and  $C_6H_5GeCl_3-NH_3$  are rotated about the torsional coordinate by  $18^\circ$  and  $14^\circ$ , respectively. In addition, for  $C_6H_5SiF_3-NH_3$ ,  $C_6H_5SiCl_3-NH_3$ , and  $C_6H_5GeCl_3-NH_3$ , the  $NH_3$  is tilted toward the adjacent C-H bond of the phenyl ring in a manner that suggests a weak hydrogen bonding interaction (C-H--N). However, the distances in all three of these weaker phenyl-containing systems are much shorter than those of their methyl

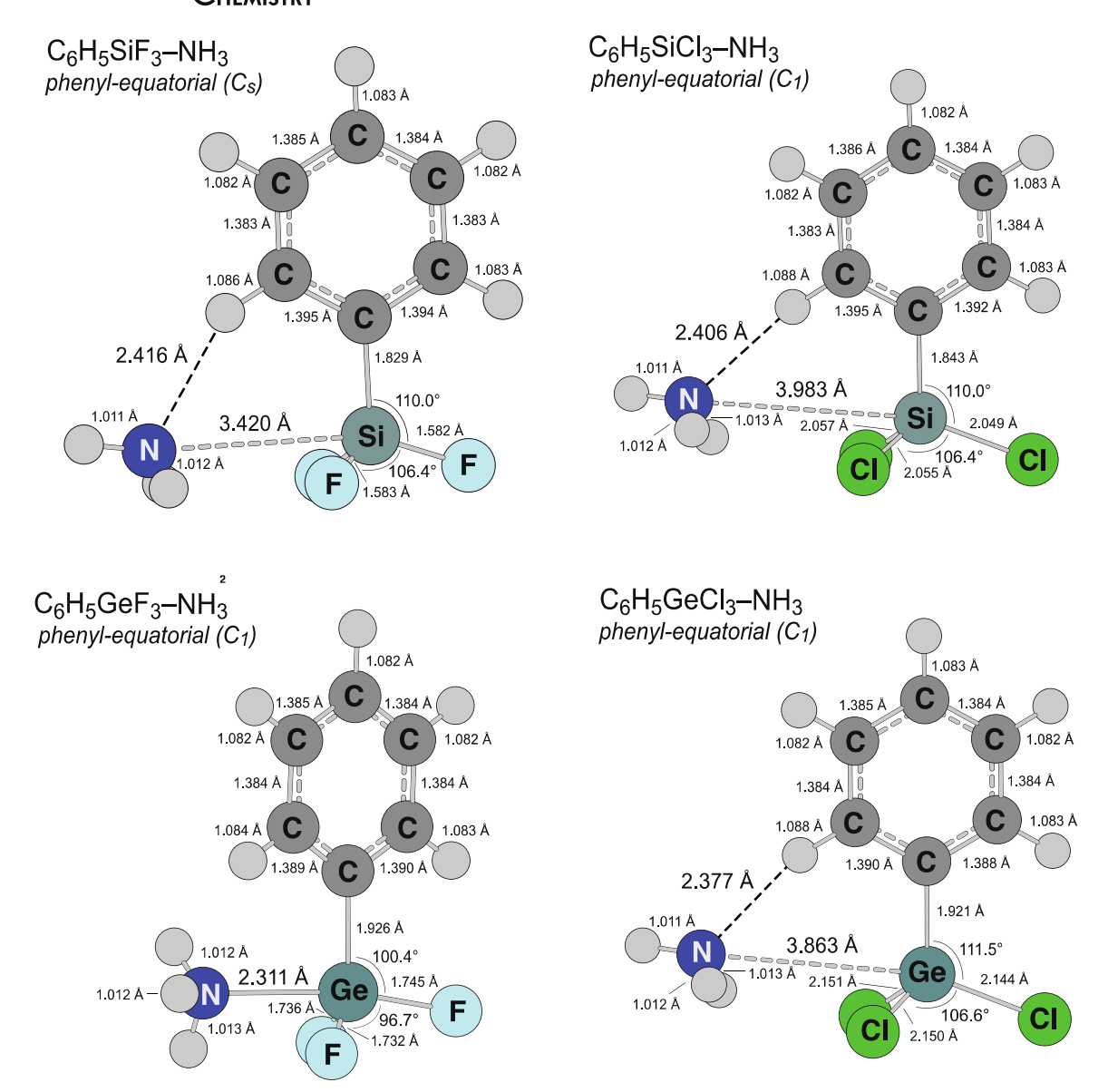


**FIGURE 3** Minimum-energy, phenyl-equatorial structures  $C_6H_5MX_3-NH_3$  complexes via M06/aug-cc-pVTZ. The  $C_6H_5SiCl_3-NH_3$  and  $C_6H_5GeCl_3-NH_3$  complexes exhibit slight deviations from  $C_5$  symmetry; in addition to the minor bond length differences noted, the NH<sub>3</sub> subunit is tilted such that the upper-left N-H bond is rotated forward, out of the plane of the page

counterparts. All are close to 2.4 Å, which is about 0.4 Å shorter than the predicted van der Waals contact distance. This, together with the extremely long Si-N and Ge-N distances, indicates that hydrogen bonding likely comprises the primary interactions in these systems. For  $C_6H_5SiCl_3-NH_3$  and  $C_6H_5GeCl_3-NH_3$ , the N-Si and N-Ge distances (3.983 and 3.863 Å, respectively) are over 0.2 Å *longer* than the predicted van der Waals contact distances (3.65 Å). We also note that the situation with  $C_6H_5SiF_3-NH_3$  seems to parallel the other weak phenyl complexes, rather than its methyl counterpart in Figure 2. Here, the N-H distance (2.416 Å) is comparable to those in the  $C_6H_5MCl_3$  systems and is again on par with sum of the N and H van der Waals radii. This, together with an N-Si distance that is about 0.2 Å longer than its methyl counterpart, and perhaps a bit less distortion in the acid subunit, suggest that hydrogen bonding along the C-H--N linkage may be the primary interaction here as well. It is also worth noting that we did locate secondary minima for  $C_6H_5SiF_3-NH_3$ ,  $C_6H_5SiCl_3-NH_3$ , and  $C_6H_5GeCl_3-NH_3$  that had shorter M-N distances and lacked any such hydrogen bonding interaction due to a tilt in the phenyl ring, which rendered the C-H bond inaccessible. However, these geometries were all about a kcal/mol higher in energy than the structures displayed in Figure 3.

The fairly strong  $C_6H_5GeF_3-NH_3$  complex is the outlier relative to its phenyl-containing counterparts, and its structure parallels that of its methyl analog, with a short Ge-N distance (2.311 Å) and a moderately large binding energy (9.4 kcal/mol). The acid fragment is significantly distorted, with bond angles of 96.7 and  $100.4^{\circ}$ , intermediate between the ideal tetrahedral and trigonal bipyramidal values, once again suggesting an interaction best described as "intermediate". In addition, the NH<sub>3</sub> is only approximately staggered with respect to the acid fragment; it is tilted by

**TABLE 3** Thermochemical data for R-equatorial isomers of RMX<sub>3</sub>-NH<sub>3</sub><sup>a</sup>

| Complex  | $\Delta E^b$ | $\Delta E_{ZPT}^{b}$ | $\Delta H^c$ | $\Delta G^c$ |
|--|--------------|----------------------|--------------|--------------|
| CH <sub>3</sub> SiF <sub>3</sub> -NH <sub>3</sub>  | -4.6         | -3.7                 | -3.4         | 2.6          |
| CH <sub>3</sub> SiCl <sub>3</sub> -NH <sub>3</sub> | -4.2         | -3.1                 | -2.9         | 3.7          |
| $CH_3GeF_3$ - $NH_3$                               | -8.9         | -6.6                 | -7.1         | 1.6          |
| CH <sub>3</sub> GeCl <sub>3</sub> -NH <sub>3</sub> | -5.2         | -4.1                 | -3.9         | 2.5          |
| $C_6H_5SiF_3-NH_3$                                 | -4.7         | -3.3                 | -3.2         | 4.7          |
| $C_6H_5SiCl_3-NH_3$                                | -3.9         | -3.0                 | -2.6         | 4.2          |
| $C_6H_5GeF_3$ - $NH_3$                             | -9.4         | -6.9                 | -7.5         | 3.6          |
| $C_6H_5GeCl_3-NH_3$                                | -4.7         | -3.6                 | -2.9         | 3.5          |

<sup>&</sup>lt;sup>a</sup>Units of kcal/mol.

about 23° (such that the lower N-H bond in Figure 3 points into the plane of the page). In addition, the phenyl ring is tilted by about 37° relative to the plane defined by the  $F_{axial}$ -Si- $C_a$  linkage (the left side of the ring as pictured in Figure 3 would extend out of the plane of the page).

Despite the variability in the modes of interaction across this family of systems, there are some reasonably clear general trends in strength. Two general observations are that the binding energies are significantly offset by the zero-point energy corrections, and in addition, the Gibbs energy changes for the formation of the complexes are all positive. As a whole, the Ge-containing complexes are stronger than their silicon analogs, by about 1 kcal/mol in the case of the X=Cl compounds and by 4 to 5 kcal/mol in the case of the X=F compounds. Similarly, the fluorine-containing systems are stronger than their chloro counterparts by about 0.5 to 1.0 kcal/mol in the case of M=Si and by about 4 to 5 kcal/mol in the case of M=Ge. The effect of the R-group is quite subtle and manifests differences in binding energy of only 0.1 to 0.5 kcal/mol. In the case of the X=F systems, the R=Ch<sub>3</sub> complexes are somewhat more strongly bound, and in the case of the X=Cl systems, the R=CH<sub>3</sub> complexes are slightly stronger.

These strength (ie, binding energy) trends, however, do not always parallel structural data such as the M-N distances in a manner expected for donor-acceptor systems—this is further evidence that weak hydrogen bonding makes significant contributions to the overall interaction energies. Case in point, here are the X=Cl systems in which the  $R=C_6H_5$  analogs have significantly longer M-N distances than their  $R=CH_3$  counterparts but have larger binding energies and much shorter C-H--N distances. These observations are quite consistent with the predominance of the hydrogen-bonding interactions over any sort of tetrel-bonding interaction between the  $NH_3$  and the metal center. However, the fact that both M=Ge systems have shorter M-N distances than their M=Si analogs does argue for some sort of composite interaction. A similar situation arises upon a comparison of  $CH_3SiF_3$ - $NH_3$  and  $C_6H_5SiF_3$ - $NH_3$ , in which the binding energy of the former is smaller (albeit by only 0.1 kcal/mol), but its Si-N distance is a full 0.2 Å shorter. However, this too can be rationalized by considering hydrogen-bonding interactions within the C-H--N linkage, which seem to be secondary for  $CH_3SiF_3$ - $NH_3$  (shorter N-Si distance, smaller binding energy) but more dominant in  $C_6H_5SiF_3$ - $NH_3$  (longer N-Si distance, large binding energy).

One additional point of comparison is how the strengths of these complexes compare to their  $MX_4$  counterparts, an illustration of how replacing a single halogen with an organic substituent affects acceptor strength. The M06/aug-cc-pVTZ binding energies of the NH<sub>3</sub> complexes of SiF<sub>4</sub>, SiCl<sub>4</sub>, GeF<sub>4</sub>, and GeCl<sub>4</sub>, which are exclusively tetrel bonded, are 9.4, 3.1, 19.7, and 5.8 kcal/mol, respectively. Among these, the SiF<sub>4</sub> and GeF<sub>4</sub> are relatively strong, and the latter most likely provides a reliable benchmark for a strong tetrel bond. In addition, they are substantially stronger than their MF<sub>3</sub>R counterparts by about 5 kcal/mol and about 10 kcal/mol for H<sub>3</sub>N-SiF<sub>4</sub> and H<sub>3</sub>N-GeF<sub>4</sub>, respectively. This indicates that the addition of the R group substantially reduces the Lewis acidity of these M=F compounds. However, the situation with H<sub>3</sub>N-SiCl<sub>4</sub> and H<sub>3</sub>N-GeCl<sub>4</sub> is quite peculiar. In these cases, the binding energies are within about 1 kcal/mol of their MCl<sub>3</sub>R counterparts, and in fact, the binding energy of H<sub>3</sub>N-SiCH<sub>3</sub>Cl<sub>3</sub> just slightly *exceeds* that of H<sub>3</sub>N-SiCl<sub>4</sub>. One factor is apparently that the X=Cl compounds are much weaker acceptors than their X=F counterparts, but any trend may also be obscured by differences in the nature of the interactions in the MCl<sub>4</sub> and MCl<sub>3</sub>R complexes—tetrel vs hydrogen bonding, respectively.

## 3.3 | Metastable "R-axial" structures

In addition to the global-minimum R-equatorial structures, we also identified a set of metastable R-axial structures, which are depicted in Figures 4 and 5 for the methyl and phenyl compounds, respectively, and corresponding thermochemical data are presented in Table 4. These structures may be inaccessible from an experimental standpoint, but they do illustrate the applicability of the sigma-hole model to these compounds with distinctly different bonding sites. Furthermore, as we move forward with this line of research, we will be seeking complexes for which the R-axial

<sup>&</sup>lt;sup>b</sup>Energy difference between complex and sum of isolated fragments, "ZPT" refers to the zero-point energy-corrected value.

 $<sup>^{</sup>c}\Delta H$  and  $\Delta G$  relative to isolated fragments at 298 K.

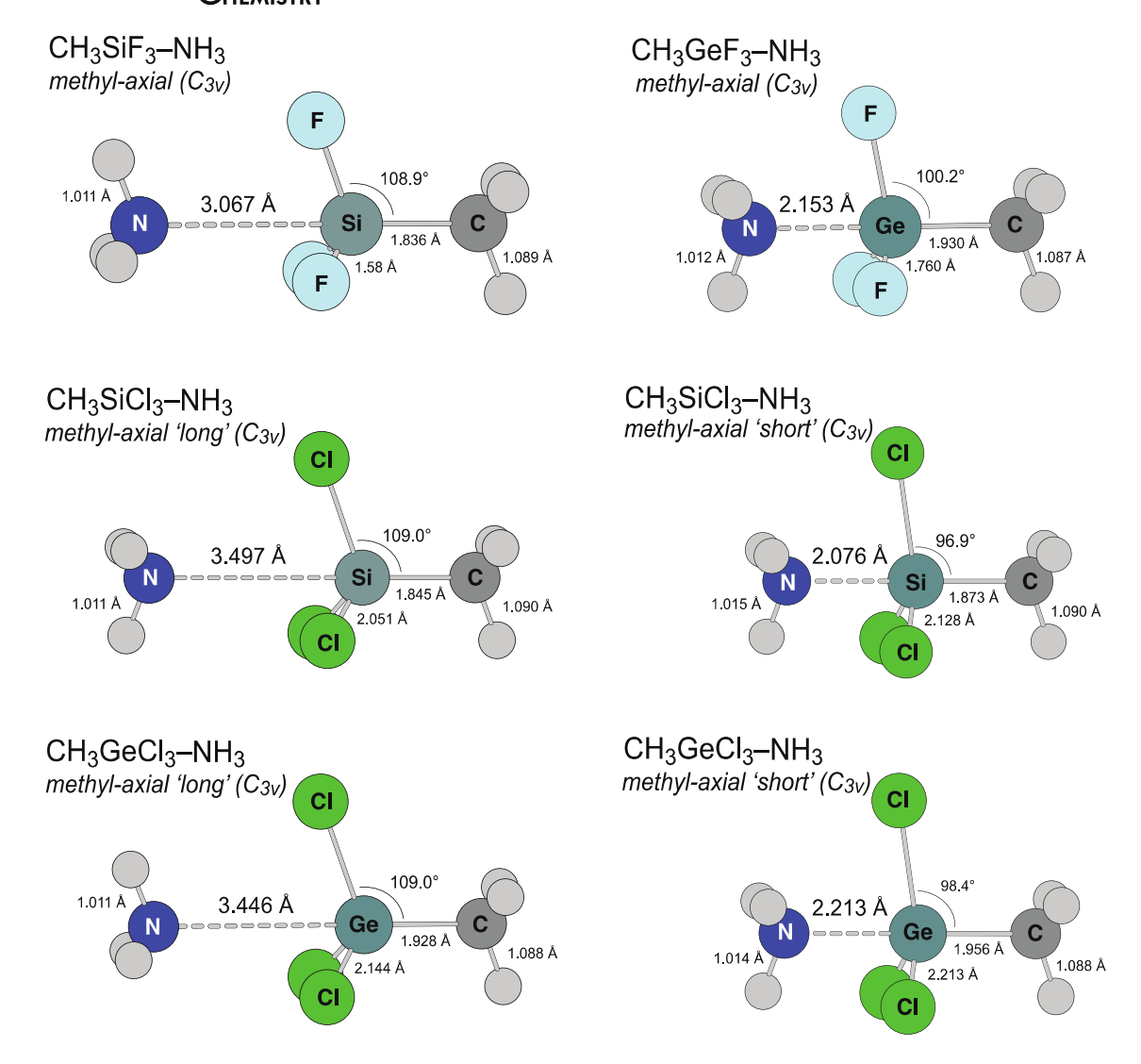


**FIGURE 4** Metastable, methyl-axial structures for CH<sub>3</sub>MX<sub>3</sub>-NH<sub>3</sub> complexes via M06/aug-cc-pVTZ. These structres are symmtrical and exhbit all real frequencies. See text for discussion

configuration is most stable, and the sigma-hole concept will guide us in that effort. In any event, these R-axial structures are all true minima with all real frequencies. To some extent, these structures fall into two classes: those with fairly short or fairly long M-N interaction distances. In fact, the  $CH_3SiCl_3-NH_3$  and  $CH_3GeCl_3-NH_3$  systems exhibit two distinct R-axial structures with distinctly different M-N bond distances, a phenomenon we have encountered before in our studies of nitrile-BCl<sub>3</sub> complexes. [39,40] For the most part, these structures lie 2 to 3 kcal/mol above the respective R-equatorial structures. The exceptions are the short-bond forms of the RMCl<sub>3</sub>-NH<sub>3</sub> complexes, which lie about 4 to 6 kcal/mol above their R-equatorial counterparts.

The structures with relatively long M-N distances are displayed on the left in Figures 4 and 5, and these include the "long-bond" forms of the RSiCl<sub>3</sub>-NH<sub>3</sub> and RGeCl<sub>3</sub>-NH<sub>3</sub> systems, as well as the RSiF<sub>3</sub>-NH<sub>3</sub> complexes. For the most part, these structures reflect weak N $\rightarrow$ M tetrel interactions, in which the acid fragments remain largely undistorted. For CH<sub>3</sub>SiCl<sub>3</sub>-NH<sub>3</sub> and CH<sub>3</sub>GeCl<sub>3</sub>-NH<sub>3</sub>, the M-N distances systems are about 0.15 to 0.20 Å shorter than the expected van der Waals contact (3.65 Å for Si-N, 3.66 Å for Ge-N), and binding energies are -2.5 and 2.0 kcal/mol, respectively. C<sub>6</sub>H<sub>5</sub>SiCl<sub>3</sub>-NH<sub>3</sub> and C<sub>6</sub>H<sub>5</sub>GeCl<sub>3</sub>-NH<sub>3</sub> appear to be slightly weaker systems; the M-N distances are longer, very near the predicted van der Waals contact value, and the binding energies are lower (1.7 and 2.0 kcal/mol, respectively). In addition, in these systems, the NH<sub>3</sub> subunit it tiled in a manner that seems to align its dipole with one of the M-Cl bonds, thereby disfavoring the tetrel interaction. The RSiF<sub>3</sub>-NH<sub>3</sub> complexes exhibit N-Si distances close to 3.0 Å, about 0.5 Å lower than the predicted van der Waals contact, and binding energies of about 2.5 kcal/mol. In addition, these distances are 0.2 and 0.4 Å shorter than in the global-minimum R-equatorial structures for the methyl and phenyl complexes, respectively, in spite of the binding energies that are lower by 2 kcal/mol. The reason for this is not clear, but it is consistent with a significant hydrogen-bonding contribution to the interaction energies in the R-equatorial forms of these complexes.

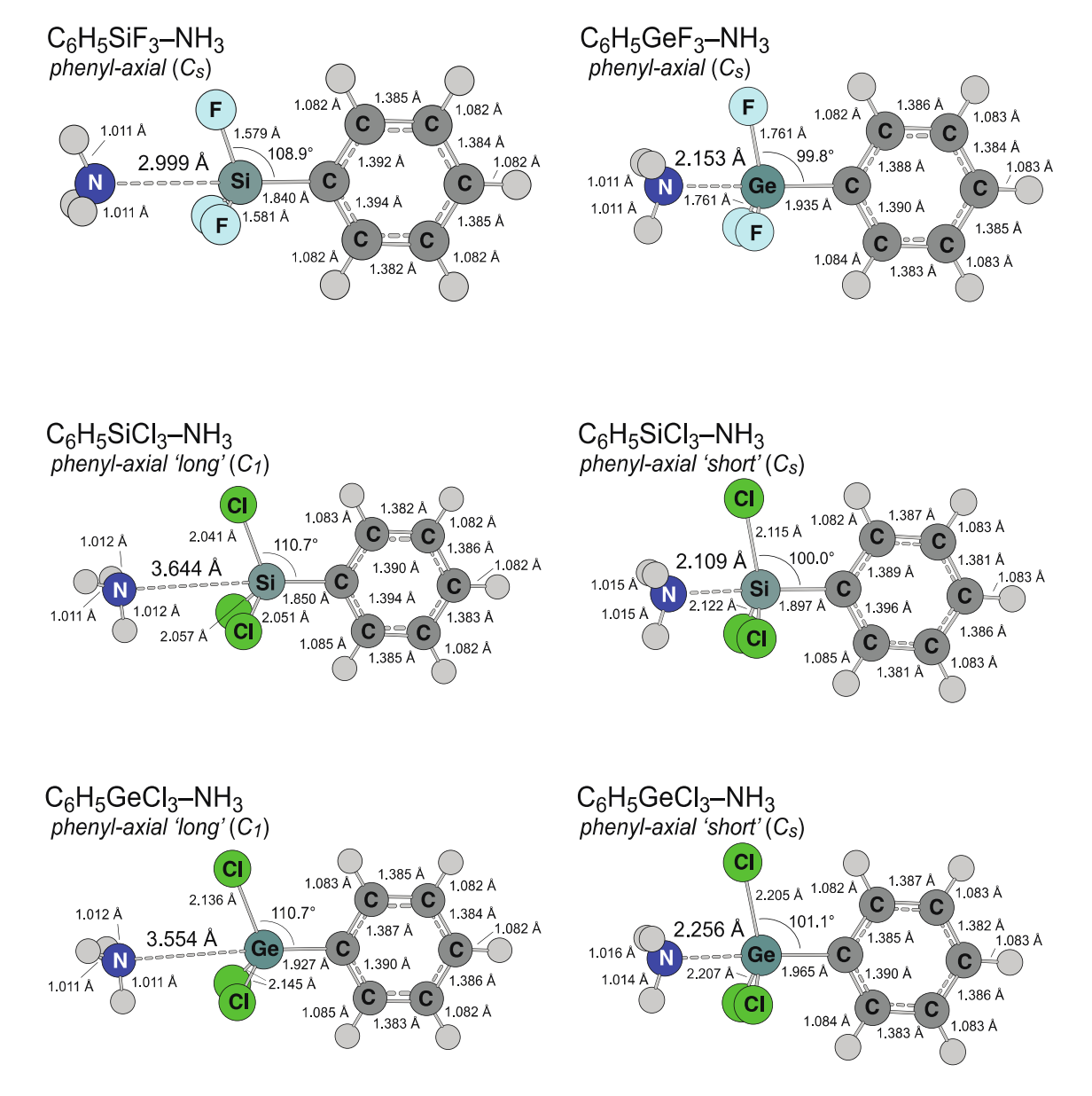


**FIGURE 5** Metastable, phenyl-axial structures for  $C_5H_6MX_3-NH_3$  complexes via M06/aug-cc-pVTZ. For the long-bond forms of  $C_6H_5MCl_3-NH_3$  (lower left), the NH<sub>3</sub> is tilted inward in a manner that partially aligns its  $C_3$  axis with the M-Cl bond projecting into the page

The structures with relatively short M-N distances are displayed on the right in Figures 4 and 5, and these consist of the RGeF<sub>3</sub>-NH<sub>3</sub> complexes and the short-bond forms of the RSiCl<sub>3</sub>-NH<sub>3</sub> and RGeCl<sub>3</sub>-NH<sub>3</sub> systems. The RGeF<sub>3</sub>-NH<sub>3</sub> structures are quite similar and reflect moderately strong N $\rightarrow$ M tetrel interactions with fairly short Ge-N distances (2.153 Å), a significant degree of distortion in the acid fragments, and moderately large binding energies (7.9 kcal/mol). Like their silicon counterparts, the M-N distances are shorter than in the R-equatorial forms in spite of the weaker binding. The short-bond forms of the RSiCl<sub>3</sub>-NH<sub>3</sub> and RGeCl<sub>3</sub>-NH<sub>3</sub> complexes exhibit notably short M-N bonds, over 1.0 Å shorter than their long-bond counterparts, and a significant distortion of the acid fragments. However, each of these short-bond structures is higher in energy than its long-bond analog, although in the case of CH<sub>3</sub>GeCl<sub>3</sub>-NH<sub>3</sub>, the difference is only 0.6 kcal/mol. In fact, C<sub>6</sub>H<sub>5</sub>SiCl<sub>3</sub>-NH<sub>3</sub> lies 1.7 kcal/mol above the separated fragments.

## 3.4 | Charge analyses

The seemingly peculiar aspects of the bonding in these systems, including the apparent preference for weak hydrogen bonding over  $N \rightarrow M$  tetrel interactions, are laid bare in an assessment of the charge distribution across this full series of RMX<sub>3</sub>-NH<sub>3</sub>compounds. Table 5 displays key

| Complex  | $\Delta E^b$ | E <sub>rel</sub> c | $\Delta E_{ZPT}^{b}$ | $\Delta H^d$ | $\Delta G^d$ |
|--|--------------|--------------------|----------------------|--------------|--------------|
| CH <sub>3</sub> SiF <sub>3</sub> -NH <sub>3</sub>                        | -2.5         | 2.2                | -1.7                 | -1.3         | 4.4          |
| CH <sub>3</sub> SiCl <sub>3</sub> -NH <sub>3</sub> (short)               | -0.1         | 4.2                | 3.5                  | 2.4          | 13.6         |
| $CH_3SiCl_3-NH_3$ (long)   | -1.7         | 2.5                | -0.9                 | -0.4         | 6.2          |
| CH <sub>3</sub> GeF <sub>3</sub> -NH <sub>3</sub>                        | -7.9         | 1.0                | -5.2                 | -5.9         | 4.3          |
| CH <sub>3</sub> GeCl <sub>3</sub> -NH <sub>3</sub> (short)               | -1.4         | 3.8                | 1.6                  | 0.8          | 11.5         |
| $CH_3GeCl_3-NH_3$ (long)   | -2.0         | 3.2                | -1.4                 | -0.8         | 4.9          |
| C <sub>6</sub> H <sub>5</sub> SiF <sub>3</sub> -NH <sub>3</sub>          | -2.6         | 2.0                | -1.7                 | -1.4         | 4.8          |
| C <sub>6</sub> H <sub>5</sub> SiCl <sub>3</sub> -NH <sub>3</sub> (short) | 1.7          | 5.6                | 4.8                  | 3.9          | 14.3         |
| $C_6H_5SiCl_3-NH_3(long)$  | -1.7         | 2.2                | -0.9                 | -0.5         | 6.2          |
| C <sub>6</sub> H <sub>5</sub> GeF <sub>3</sub> -NH <sub>3</sub>          | -7.9         | 1.5                | -5.1                 | -5.8         | 5.7          |
| C <sub>6</sub> H <sub>5</sub> GeCl <sub>3</sub> -NH <sub>3</sub> (short) | -0.2         | 4.5                | 2.7                  | 2.0          | 12.3         |
| C <sub>6</sub> H <sub>5</sub> GeCl <sub>3</sub> -NH <sub>3</sub> (long)  | -2.0         | 2.7                | -1.2                 | -0.3         | 4.8          |

**TABLE 4** Thermochemical data for R-axial isomers of RMX<sub>3</sub>-NH<sub>3</sub><sup>a</sup>

 $<sup>^{\</sup>rm d}\Delta H$  and  $\Delta G$  relative to isolated fragments at 298 K.

|   | NBO charg | NBO charge/e |                        |      | Maximum | ESP/au <sup>b</sup> |
|---|-----------|--------------|------------------------|------|---------|---------------------|
| Fragment  | н         | М            | Х                      | μ/D  | *M-R    | *M-X                |
| CH <sub>3</sub> SiF <sub>3</sub>                | 0.25      | Si: 2.36     | F: -0.64               | 2.45 | 0.029   | 0.044               |
| SiCl <sub>3</sub> CH <sub>3</sub>               | 0.25      | Si: 1.46     | Cl: -0.36              | 1.94 | 0.009   | 0.027               |
| CH₃GeF₃   | 0.25      | Ge: 2.23     | F: -0.64               | 3.8  | 0.021   | 0.055               |
| $CH_3GeCl_3$                                    | 0.25      | Ge: 1.36     | Cl: -0.36              | 2.63 | 0.009   | 0.034               |
| C <sub>6</sub> H <sub>5</sub> SiF <sub>3</sub>  | 0.20(1)   | Si: 2.38     | <sup>c</sup> F: -0.64  | 3.2  | 0.028   | 0.039               |
|   |           |              | -0.64                  |      |         |                     |
| C <sub>6</sub> H <sub>5</sub> SiCl <sub>3</sub> | 0.20(1)   | Si: 1.49     | <sup>d</sup> Cl: -0.35 | 2.71 | 0.006   | 0.016               |
|   |           |              | -0.36                  |      |         |                     |
| C <sub>6</sub> H <sub>5</sub> GeF <sub>3</sub>  | 0.20(1)   | Ge: 2.06     | <sup>c</sup> F: -0.64  | 4.94 | 0.015   | 0.049               |
|   |           |              | -0.67                  |      |         |                     |
| C <sub>6</sub> H <sub>5</sub> GeCl <sub>3</sub> | 0.20(1)   | Ge: 1.39     | <sup>d</sup> Cl: -0.35 | 3.6  | 0.005   | 0.022               |
|   |           |              | -0.35                  |      |         |                     |
|   |           |              |                        |      |         |                     |

**TABLE 5** Key charge distribution parameters for acid fragments<sup>a</sup>

parameters related to the charge distributions of the acid fragments, including NBO charges at the M and X centers, dipole moments, and maximum values of the electrostatic potential on the isodensity surfaces (0.001 au) in the sigma-hole regions opposite the X and R substituents.

One clear thing to note is that the computed point charges at M and X are relatively insensitive to the identity of R. The exception is  $CH_3GeF_3$  relative to  $PhGeF_3$ , in which the metal center is slightly less positive in the latter case (2.06e vs 2.23e), an indication that the phenyl group does release some additional electron density relative to methyl. In addition, charge saturation appears to be achieved by the F and Cl centers on both Si and Ge compounds; the charges on F and Cl are consistently -0.64e and -0.35(1)e, respectively. However, the charge transfer from M to the X centers is noticeably higher for X=F than for X=Cl, such that the M centers in the fluoride molecules have a higher positive charge by roughly 0.7e to 0.9e. In addition, the dipole moments of the fluorides are higher as well, by about 0.5 D for M=Si and by 1.2 to 1.3 D for M=Ge.

Again, as was noted above, the identity of R has little or no effect on the charges at the M and X centers, RGeF<sub>3</sub> compounds notwithstanding, but there are some differences between the methyl and phenyl systems. For one, the phenyl compounds have much larger dipole moments,

<sup>&</sup>lt;sup>a</sup>Units of kcal/mol.

<sup>&</sup>lt;sup>b</sup>Energy difference between complex and sum of isolated fragments, "ZPT" refers to the zero-point energy-corrected value.

<sup>&</sup>lt;sup>c</sup>E<sub>rel</sub> is the energy relative to the corresponding R-equatorial structure.

 $<sup>^</sup>aFor\ NH_3,$  the point charges are –1.06e and 0.35e for N and H, respectively, and  $\mu$  = 1.49 D.

<sup>&</sup>lt;sup>b</sup>The maximum electrostatic potential observed in sigma-hole region (on the 0.001au isodensity surface of  $MX_3R$ ) on M opposite the M-R or M-X bonds as indicated. For  $NH_3$ , the potential extremum is -0.059 au at the lone pair on N.

<sup>&</sup>lt;sup>c</sup>Top: 30° dihedral angle; bottom: 90° dihedral angle.

<sup>&</sup>lt;sup>d</sup>Top: 0° dihedral angle; bottom: 60° dihedral angle.

by roughly 0.8 to 1.0 D. In addition, the sigma-holes (both M-R and M-X) tend to be slightly stronger in the methyl cases, as indicated by the maxima on the electrostatic potential surfaces. For the methyl-fluoro compounds, the maxima are about 0.005 au larger in magnitude than their phenyl counterparts. For the methyl-chloro compounds, the maxima are about 0.01 au larger in magnitude than their phenyl counterparts. However, these differences are minor compared to those manifested by the identity of the X or M centers.

Above all else, it is the identity of the halogens that manifests the most significant difference in the charge distribution parameters of the acid fragments and, in turn, the most significant difference in the strength of the coordinate bond to NH<sub>3</sub>. For instance, the maximum potential at Ge opposite the Ge-Cl bond (about +0.005 au) is a full order of magnitude smaller than maximum potential at Ge opposite the Ge-F sigma-holes (about +0.049 au). Thus, any potential consequence of differences in the electron-donating abilities of methyl and phenyl, for instance, are rendered negligible by the dominant electron-withdrawing power of the geminal halogen substituents on the common M center. In fact, the potentials on M opposite both the M-X and M-R bonds are significantly intensified by replacing Cl by F, and this far exceeds the effect due to R. As a whole, however, the potentials M opposite the M-C bonds for both phenyl and methyl are substantially lower than those opposite the M-X bonds, even when the methyl substituent induces a small but consistently more positive potential than phenyl. An apparent consequence of the disparity in the strengths of the sigma-holes opposite the M-X and the M-R bonds is that complexes with the base axial to the M-R bonds are consistently less stable than the alternative systems with the base axial to the M-X bond. This is so even though the latter systems have consistently longer M-N contacts, which is explained, in part, by the prevalence of hydrogen bonding in some of the R-equatorial structures. However, even for H<sub>3</sub>N-GeF<sub>3</sub>CH<sub>3</sub>, the R-equatorial geometry with NH<sub>3</sub> axial to the Ge-F bond has a Ge-N distance that is over 0.20 Å longer, but the binding energy exceeds that if the R-axial structure by 2.0 kcal/mol.

Maps of the electrostatic potentials for the fluorine-containing acid fragments—plotted on a common scale for the case of the most extreme potentials—are shown in Figure 6. The structures are oriented such that the halides are at the top, with one pointing into the plane of the paper. The structures are tilted such that the slightly positive potentials opposite the R groups are visible at the top of the maps, while those due to the halide (on the backside of each structure) are front and center (see annotations). Above, we noted a remarkable observation that, for most of the weaker, R-equatorial structures, a C-H--N hydrogen bonding interaction seems to predominate over direct coordination to the metal center. These potential maps in Figure 6 relieve us of any anxiety about this outcome. Certainly, for the chlorine-containing fragments (right), which are most clearly hydrogen-bonded in the R-equatorial forms, the potentials on the H centers are the most positive (blue), more so than either sigmahole region. At the other extreme,  $CH_3GeF_3$  and  $C_6H_5GeF_3$  (bottom left) exhibit distinctly positive regions for the sigma-holes opposite the Ge-F bond, and these fragments form moderately strong  $N \rightarrow Ge$  tetrel bonds with  $NH_3$ . The  $CH_3SiF_3$  and  $C_6H_5SiF_3$  cases are less clear as the blue

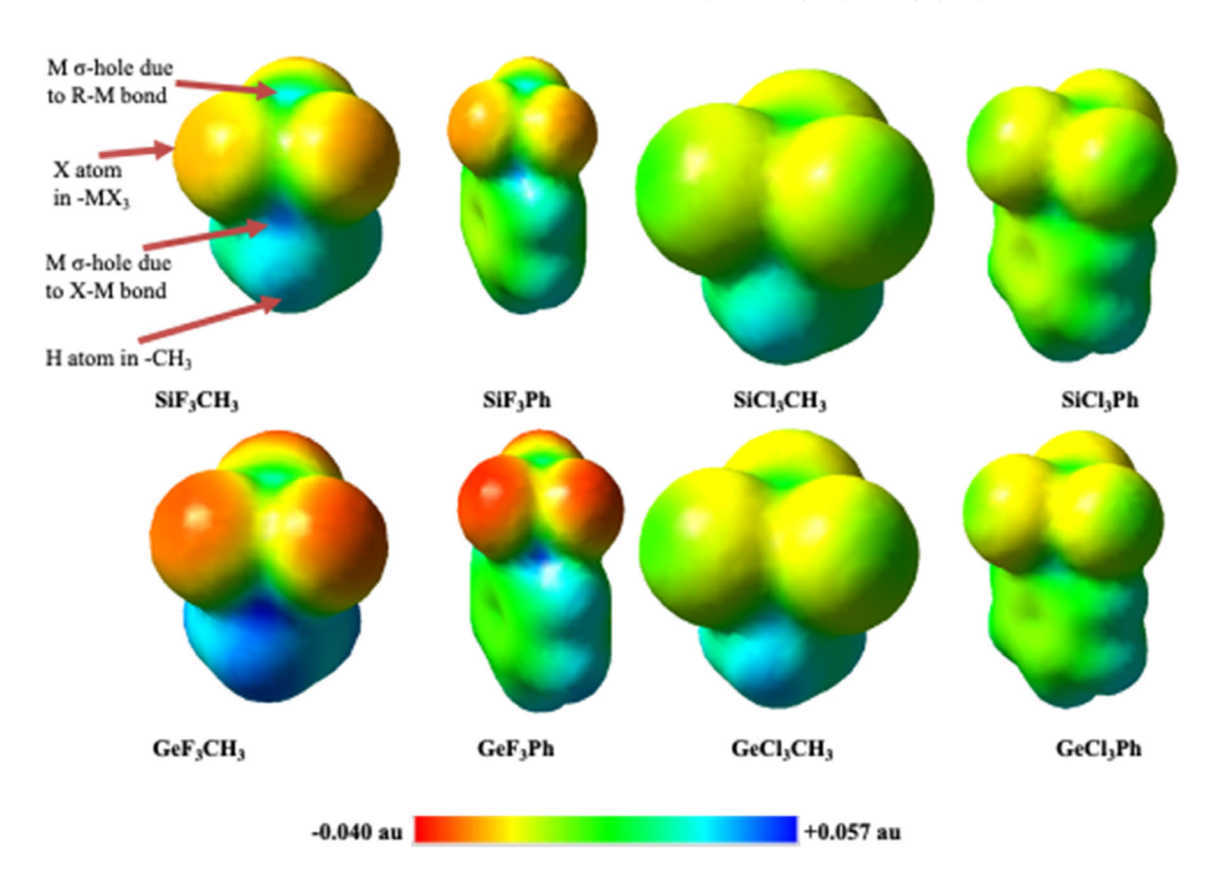


**FIGURE 6** Electrostatic potential maps for the acid fragment ( $MX_3R$ ) systems. The maps are all plotted on a common scale (spanning potentials of +0.0566 au (blue) to -0.0400 au (red)) on the 0.001 au isodensity surface

(positive) regions about the hydrogens and the \*M-X sigma-hole are comparable, perhaps slightly favoring the latter. In turn, the interactions with the NH<sub>3</sub> subunit in the complexes are less distinct, with the bond axis of the NH<sub>3</sub> fragment pointing between the C-H bond and the metal center, perhaps a compromise between the tetrel (N $\rightarrow$ Si) and H-bond (C-H--N) interactions.

# 3.5 | Matrix IR spectra

We obtained infrared spectra of cryogenic argon matrices seeded with NH<sub>3</sub> and CH<sub>3</sub>SiCl<sub>3</sub> or CH<sub>3</sub>GeCl<sub>3</sub> and ultimately found that the observed patterns of the product bands (those that are observed to only have the presence of both complexes subunits) were consistent with the presence of the methyl-equatorial form of CH<sub>3</sub>SiCl<sub>3</sub>-NH<sub>3</sub> but less conclusive in the case of CH<sub>3</sub>GeCl<sub>3</sub>-NH<sub>3</sub>. We note here that these spectra were difficult to interpret due to weak product-band signals that were shifted only slightly from the corresponding fragment bands. This was particularly problematic in the case of CH<sub>3</sub>GeCl<sub>3</sub> experiments because of the presence of five naturally abundant Ge isotopes, which significantly broadens most of the fragment bands. Typically, matrix-IR spectra are assigned though a meticulous analysis of peak areas, undertaken to ensure that assigned product bands exhibit consistent relative intensities across a range of conditions. Here, the product bands reported were only observed in a narrow range of near-optimal conditions, and peak area measurements were unreliable due to overlap with the relatively strong fragment bands. However, the validated M06 frequency predictions make a compelling case for the presence of the R-equatorial forms of the complexes, especially for CH<sub>3</sub>SiCl<sub>3</sub>-NH<sub>3</sub>, even in the absence of rigorously confirmed band assignments.

In matrices seeded with NH<sub>3</sub> and CH<sub>3</sub>SiCl<sub>3</sub>, we observed product bands at 566/567, 765, 810/816, and 1048 cm<sup>-1</sup>, the first three of which are shifted only slightly from the following peaks observed for the CH<sub>3</sub>SiCl<sub>3</sub> fragment: The Si-Cl asymmetric stretch at 575 cm<sup>-1</sup>, the Si-C stretch at 761 cm<sup>-1</sup>, and the CH<sub>3</sub> wag at 799 cm<sup>-1</sup>. The other (1048 cm<sup>-1</sup>) lies in the region of the NH<sub>3</sub> "umbrella" motion. We note that pairs of frequency values separated by "/" (eg, 566/567) signify doublets, either due to nearly degenerate modes and/or matrix site splittings. A comparison of these observed product bands and the corresponding M06/aug-cc-pVTZ predictions for the three predicted structures of CH<sub>3</sub>SiCl<sub>3</sub>-NH<sub>3</sub> is presented in Table 6. The predictions for methyl-equatorial geometry clearly provide the best agreement with the experimental frequencies, and that agreement is striking. The shifts predicted for the short form of the R-axial structure are extreme in at least two of three cases, and for the long form of the R-axial structure, the predicted shifts are slight but in the opposite direction from what is observed. Often, matrix-IR assignments

|                           | Si-Cl assy stretch |                    | Si-C stretch |                    | CH <sub>3</sub> Wag |                    |
|---------------------------|--------------------|--------------------|--------------|--------------------|---------------------|--------------------|
| Mode:                     | Freq <sup>b</sup>  | Shift <sup>c</sup> | Freq         | Shift <sup>c</sup> | Freq <sup>b</sup>   | Shift <sup>c</sup> |
| Experimental <sup>d</sup> | 567/566            | (-8/-9)            | 765          | (+4)               | 810/816             | (+11/+15)          |
| R-equatorial (M06)        | 566/564            | (-7/-9)            | 764          | (+5)               | 808/823             | (+6/+23)           |
| R-axial long (M06)        | 576                | (+ 3)              | 747          | (-12)              | 799/800             | (-1/0)             |
| R-axial short (M06)       | 500                | (-73)              | 700          | (-59)              | 826/827             | (+26/+27)          |

**TABLE 6** A comparison of observed and predicted frequencies<sup>a</sup> for CH<sub>3</sub>SiCl<sub>3</sub>-NH<sub>3</sub>

<sup>&</sup>lt;sup>d</sup>Observed product bands in argon matrices seeded with CH<sub>3</sub>SiCl<sub>3</sub> and NH<sub>3</sub>.

|                           | Ge-Cl Assy Stretch |                    | Ge-C St | retch              | CH <sub>3</sub> Wag |                    |
|---------------------------|--------------------|--------------------|---------|--------------------|---------------------|--------------------|
| Mode:                     | freq <sup>b</sup>  | shift <sup>c</sup> | Freq    | shift <sup>c</sup> | freq <sup>b</sup>   | shift <sup>c</sup> |
| Experimental <sup>d</sup> | _                  | _                  | 620?    | (-7)               | 830/846             | (+9/+25)           |
|                           |                    |                    |         |                    | 815?                | (-6)               |
| R-equatorial (M06)        | 426                | (-8)               | 627     | (+2)               | 815/831             | (+13/+28)          |
| R-axial long (M06)        | 434                | (O)                | 622     | (-5)               | 800                 | (-3)               |
| R-axial short (M06)       | 386                | (-48)              | 595     | (-32)              | 807/808             | (+4/+5)            |

<sup>&</sup>lt;sup>a</sup>Units of cm-1.

**TABLE 7** A comparison of observed and predicted frequencies<sup>a</sup> for CH<sub>3</sub>SiCl<sub>3</sub>-NH<sub>3</sub>

<sup>&</sup>lt;sup>a</sup>Units of cm-1.

<sup>&</sup>lt;sup>b</sup>Bands denoted as pairs separated by "/" are doublets due to matrix sites or slight splittings of nearlydegenerate bands; see text for discussion.

<sup>&</sup>lt;sup>c</sup>Complex induced shift:  $\nu$  (complex) –  $\nu$  (fragment) in each case.

<sup>&</sup>lt;sup>b</sup>Bands denoted as pairs separated by "/" are doublets due to matrix sites or slight splittings of nearly-degenerate bands; see text for discussion.

<sup>&</sup>lt;sup>c</sup>Complex induced shift:  $\nu$  (complex) -  $\nu$  (fragment) in each case.

<sup>&</sup>lt;sup>d</sup>Observed product bands in argon matrices seeded with CH<sub>3</sub>GeCl<sub>3</sub> and NH<sub>3</sub>.

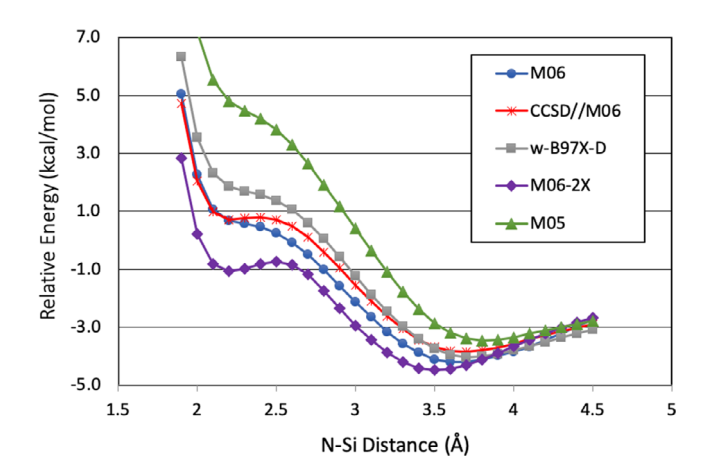
are substantiated on the basis of predicted spectra shifts, which would subtract the sometimes-large error in the absolute frequency predictions. However, in the present situation, having chosen the M06 method on the basis of the validation against the observed bands of the parent acid fragment, not only are the shifts in agreement, but the absolute frequencies agree remarkably as well. We also note that the precited value of the NH<sub>3</sub> "umbrella" frequency in the methyl-equatorial structure is 1041 cm<sup>-1</sup>, and this only differs by 7 cm<sup>-1</sup> from the observed product band in this region (despite not including NH<sub>3</sub> frequencies in our validation). Overall, these comparisons present a reasonably convincing case that the observed product bands arise from the methyl-equatorial form of the complex.

The situation for the CH<sub>3</sub>GeCl<sub>3</sub>/NH<sub>3</sub> matrix experiments is less clear, mainly because we observe only a few product bands, and they are observed in a very narrow range of conditions. These include a doublet at 830/846 cm<sup>-1</sup>, near the CH<sub>3</sub> wag band of the CH<sub>3</sub>GeCl<sub>3</sub> fragment, and a peak at 1008 cm<sup>-1</sup>, in the NH<sub>3</sub> umbrella region, as well as peaks at 620, 815, and 1037/1042 that were observed only when the sample was annealed. Nonetheless, the M06 predictions for the various forms of CH<sub>3</sub>GeCl<sub>3</sub>-NH<sub>3</sub> are displayed in Table 7, and there is good agreement between the predicted M06 shifts for the CH<sub>3</sub> wag and the pair of product bands at 830 and 846 cm<sup>-1</sup>. The peaks in the NH<sub>3</sub> umbrella region that were observed only in annealing experiments (1037/1046) also agree with M06 predictions for the methyl-equatorial form (1046 cm<sup>-1</sup>). The other peaks, which are observed only in some annealing experiments (620 and 815 cm<sup>-1</sup>), seem to agree with the predicted shift of the long-bond, methyl-axial structure, as does the 1008 cm<sup>-1</sup> peak in the NH<sub>3</sub> umbrella region, for which the M06 prediction is 1006 cm<sup>-1</sup>. These peaks, as a whole (excepting the 1008 cm<sup>-1</sup>), lack the reproducibility to make any definitive statement regarding the presence the metastable, methyl-axial structure in the matrix; however, partitioning the complexes between two forms in the sample would further impede their observation. In any event, these data remain inconclusive, the reproducible product bands at 830 and 846 cm<sup>-1</sup> peaks provide some firm evidence at evidence for the presence of the methyl-equatorial form in the argon-matrix environment.

## 3.6 | M-N potential curves

We also explored the M-N potentials of CH<sub>3</sub>SiCl<sub>3</sub>-NH<sub>3</sub> and CH<sub>3</sub>GeCl<sub>3</sub>-NH<sub>3</sub>, mainly because of the experimental results of these systems, and in our past work, the donor-acceptor potential was key to understanding and predicting condensed-phase effects on structures. In addition, because

**FIGURE 7** N-Si potential energy curves for the methyl-axial form of  $CH_3SiCl_3-NH_3$  from four DFT methods and CCSD//M06 (as indicated) with the aug-cc-pVTZ basis set. Energies are plotted relative to the energies of the isolated fragments. All structure parameters except the fixed N-Si distance were optimized at each point on the DFT curves



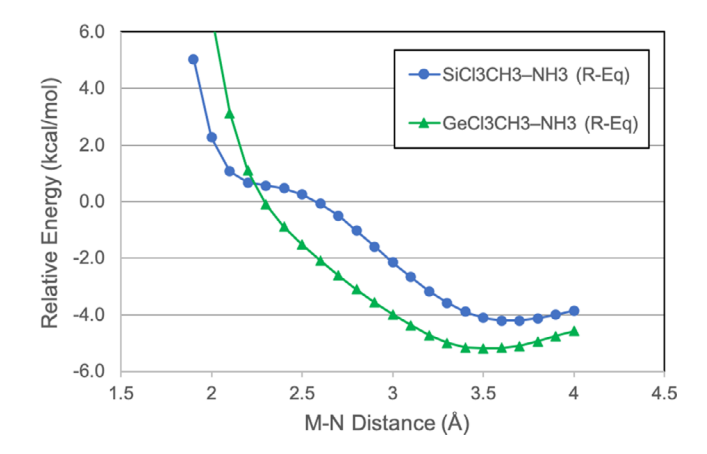


**FIGURE 8** M-N potential energy curves for the methyl-equatorial forms of CH<sub>3</sub>SiCl<sub>3</sub>-NH<sub>3</sub> and CH<sub>3</sub>GeCl<sub>3</sub>-NH<sub>3</sub>, computed via M06/aug-cc-pVTZ. Energies are plotted relative to the energies of the isolated fragments. All structure parameters except the fixed M-N distance were optimized at each point

we identified equilibrium structures with distinct M-N distances for the R-axial forms of the complexes, we elected to explore the potentials of both the methyl-equatorial and methyl-axial isomers. First, we explored the method dependence for the N-Si potential of the methyl-equatorial form of CH<sub>3</sub>SiCl<sub>3</sub>-NH<sub>3</sub>, and a collection of these curves is displayed in Figure 7. In addition to four DFT methods (M05, M06, M06-2X, and  $\omega$ B97X-D, all with the aug-cc-pVTZ basis set), we also obtained the CCSD/aug-cc-pVTZ energies of the M06 structures for reference (ie, M06//CCSD). Of the various DFT methods, M06 and  $\omega$ B97X-D track best with the CCSD energies, with M06 in slightly better agreement at the extremes of the curve and  $\omega$ B97X-D somewhat better in the intermediate region.

The M-N potentials (M06/aug-cc-pVTZ) of the methyl-equatorial forms of CH<sub>3</sub>SiCl<sub>3</sub>-NH<sub>3</sub> and CH<sub>3</sub>GeCl<sub>3</sub>-NH<sub>3</sub> are displayed in Figure 8. Clearly, both curves are quite anharmonic, with a relatively slow rise inward from the equilibrium bond length. The main difference is that there is a flat, plateau-like ridge, just inside the inner wall of the curve for CH<sub>3</sub>SiCl<sub>3</sub>-NH<sub>3</sub>, which is a feature we have seen previously in studies of MCl<sub>4</sub> complexes. <sup>[23]</sup> The curve for CH<sub>3</sub>SiCl<sub>3</sub>-NH<sub>3</sub> exhibits a long, gentle rise inward to about 2.2 Å, where the curve turns upward and the potential rises more sharply. This curve is marginally reminiscent of the weaker nitrile-BF<sub>3</sub> complexes, which are prone to substantial medium-induced changes in structure. <sup>[15,39]</sup> Another more subtle difference between the curves in Figure 8 is the onset of the predominance of the repulsive forces. Surprisingly perhaps, the repulsive region for CH<sub>3</sub>SiCl<sub>3</sub>-NH<sub>3</sub> sets in at longer bond lengths than for CH<sub>3</sub>GeCl<sub>3</sub>-NH<sub>3</sub>, until the innermost region of the curve, below about 2.2 Å. We presume the greater initial repulsion along this coordinate results from shorter M-Cl distances, which renders the Cl's in close proximity to the donor. However, as the acid fragment geometry is distorted to accommodate the donor-acceptor bond (at relatively short distances), the repulsions from these Cls are reduced. At some point, a significant portion of the repulsive interaction would stem from the metal itself, and as Ge is larger than Si, that interaction would set in at longer M-N values, and thus, at about 2.2 Å, the CH<sub>3</sub>GeCl<sub>3</sub>-NH<sub>3</sub> curve rises above that of its counterpart.

Another interesting feature, somewhat hidden in these data, is a continuous transition in the general structures of these complexes that takes place along this "tetrel-driven" coordinate, in which the binding seems to shift, continually, from an H-bond (C-H--N) to a tetrel (N $\rightarrow$ M) interaction. For CH<sub>3</sub>SiCl<sub>3</sub>-NH<sub>3</sub>, this shift takes place between 3.1 and 2.6 Å. For the transitional points in this range, the C<sub>3</sub> axis of the NH<sub>3</sub> is directed at various points along the Si-C bond, gradually shifting in its alignment from H to N through this range. At distances below 2.6 Å, the interaction is clearly tetrel in nature; the NH<sub>3</sub> lone pair is directed at the Si. The same effect occurs along the curve for CH<sub>3</sub>GeCl<sub>3</sub>-NH<sub>3</sub> but over a slightly longer distance range, 3.3 to 2.8 Å.

The M-N potentials (M06/aug-cc-pVTZ) of the methyl-axial forms of CH<sub>3</sub>SiCl<sub>3</sub>-NH<sub>3</sub> and CH<sub>3</sub>GeCl<sub>3</sub>-NH<sub>3</sub> are displayed in Figure 9. These potentials are also quite anharmonic, and the striking feature is the occurrence of two distinct minima long these curves. These were noted above as well, that is, the structures associated with these minima are displayed in Figure 4. However, these plots more readily depict the relative energies of the minima, and in addition, the barriers between them are indicated. For CH<sub>3</sub>SiCl<sub>3</sub>-NH<sub>3</sub>, the "long-bond" minimum lies about 1.5 kcal/mol, which is lower in energy, and the barrier is about 2.1 kcal/mol (relative to the outer, global minimum). In fact, the inner minimum lies just above the energy of the separated fragments. The relative energies of the two minima on the CH<sub>3</sub>GeCl<sub>3</sub>-NH<sub>3</sub> curve are much closer in energy, and the barrier is weaker. Here, the long-bond minimum lies about 0.5 kcal/mol lower in energy, and the barrier is 1.4 kcal/mol. Although these methyl-axial structures are disfavored relative to their R-equatorial counterparts, our future efforts will be concerned with designing complexes for which these arrangements are favored by incorporating more electron-withdrawing R-groups and fewer electronegative X substituents.

Finally, we explored the effect of dielectric media on the M-N potential of the R-equatorial forms of  $CH_3SiCl_3-NH_3$  and  $CH_3GeCl_3-NH_3$ , and a series of these curves for each complex is displayed in Figure 10. In each case, the top curve is the gas-phase potential (M06/aug-cc-pVTZ), and the curves below include the free energy of solvation as obtained by the PCM model (ie, PCM/M06/aug-cc-pVTZ). The sum of the gas-phase fragment energies serves as the reference in these curves. Both sets of curves exhibit, in general, the response that manifests condensed-phase structural changes in donor-acceptor systems<sup>[15]</sup>; the inner regions of the curves are preferentially stabilized, and at some

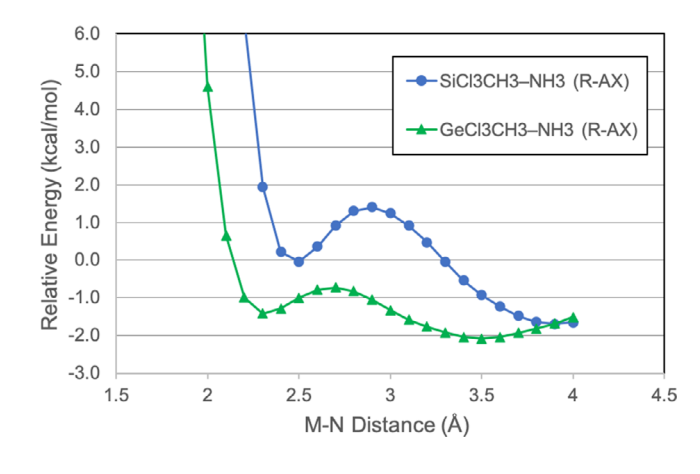


**FIGURE 9** M-N potential energy curves for the methyl-axial forms of CH<sub>3</sub>SiCl<sub>3</sub>-NH<sub>3</sub> and CH<sub>3</sub>GeCl<sub>3</sub>-NH<sub>3</sub>, computed via M06/aug-cc-pVTZ. Energies are plotted relative to the energies of the isolated fragments. All structure parameters except the fixed M-N distance were optimized at each point on the DFT curves

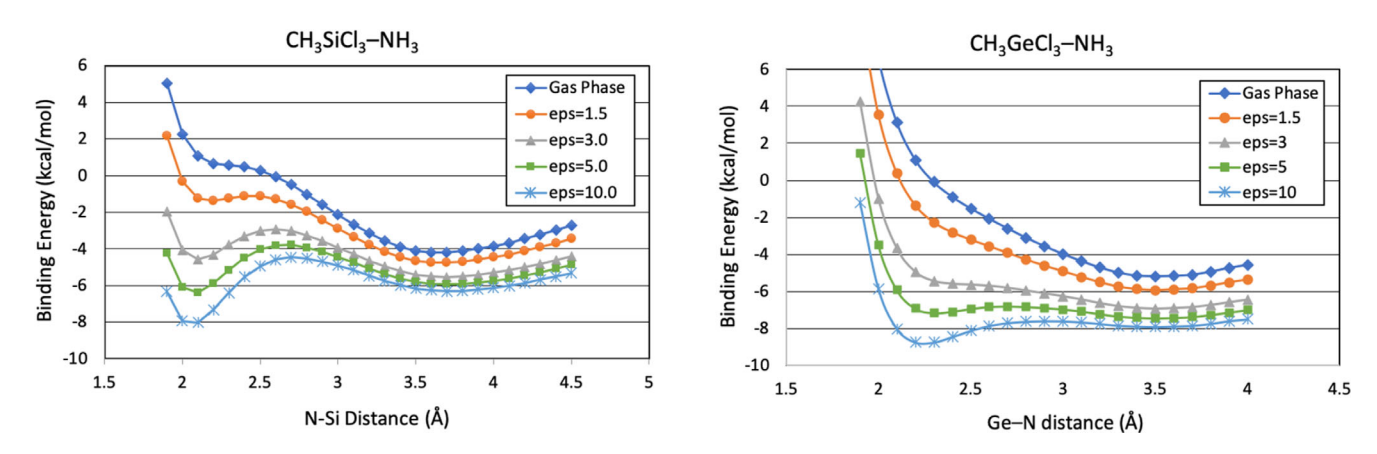


**FIGURE 10** M-N Potential energy curves for  $CH_3SiCl_3-NH_3$  and  $CH_3GeCl_3-NH_3$  in the gas phase (top) and dielectric media via (PCM/M06/aug-cc-pVTZ) computations. These energies are the sum of the gas-phase electronic energy and the solvation free energy and are plotted relative to the sum of the gas-phase fragment energies

point, the global potential minimum shifts inward. Here, the effect is slight at low dielectrics, and as noted above, we see no evidence of matrix-induced structural change. However, the key underlying behavior persists at higher dielectrics, despite the shifts in the interaction from hydrogen bonding at longer distances to tetrel bonding at shorter distances. The curves do exhibit differences however. For CH<sub>3</sub>SiCl<sub>3</sub>-NH<sub>3</sub>, the plateau-like feature becomes a distinct minimum, and it becomes the global minimum above about  $\varepsilon = 5.0$ , but the barrier persists. The curve for CH<sub>3</sub>GeCl<sub>3</sub>-NH<sub>3</sub> lacks these distinct features, but a secondary minimum develops at about 2.3 Å for  $\varepsilon$ -values above about 3.0. This minimum is global in the  $\varepsilon = 10.0$  curve, and the barrier is quite subtle. Although these data only predict a contraction of the M-N bond at high dielectrics, the general response of these potentials suggests that more sensitive systems could be designed by properly altering the substituents. [15]

#### 4 | SUMMARY AND CONCLUSIONS

We have explored the structural and energetic properties of a series of RMX<sub>3</sub>-NH<sub>3</sub> complexes (M=Si, Ge; X=F, Cl; R=CH<sub>3</sub>,  $C_6H_5$ ) using primarily M06/aug-cc-pVTZ computations, with some additional insight from matrix-isolation IR spectroscopy. The minimum-energy structures of these systems are the "R-equatorial" geometries in which the NH<sub>3</sub> binds axially to the halogen substituent, and the R-group resides in a equatorial site about the metal. However, with the exception of RGeF<sub>3</sub>-NH<sub>3</sub>, these complexes are weak, with binding energies of about 4 to 5 kcal/mol, and the acid fragments retain near-tetrahedral geometries of the complexes. Furthermore, the primary interactions in the weaker systems, especially for RMCl<sub>3</sub>-NH<sub>3</sub>, seem to be weak H-bonds between the NH<sub>3</sub> and a hydrogen on the organic substituent (C-H--N). In contrast, the RGeF<sub>3</sub>-NH<sub>3</sub> systems exhibit moderately strong tetrel bonds (N $\rightarrow$ Ge), with binding energies of about 9 kcal/mol and significant distortion of the acid subunit. Charge analyses and electrostatic potential maps of the acid fragments provide a clear rationalization of these observations; the NH<sub>3</sub> coordinates to the most positively charged region of the fragment in each of these minimum-energy cases.

We have also located meta-stable R-axial geometries for these systems, in which both the  $NH_3$  and R-groups are oriented in an axial manner. These lie between 2 and 6 kcal/mol higher in energy than their R-equatorial counterparts, and the interactions are primarily of a weak tetrel type  $(N\rightarrow M)$ . The charge analyses and fragment electrostatic potentials also provide a sound physical rationale for these observations; the sigma-holes opposite the M-R bonds are less positively charged than those opposite the M-X bonds (or the Hs on the organic group, as appropriate). One other notable feature of the R-axial geometries, in the case of in the chlorine-containing complexes, is the occurrence of distinct structures with different M-N bond distances.

Product bands observed in the IR spectra of argon matrices doped with CH<sub>3</sub>SiCl<sub>3</sub> and NH<sub>3</sub> are quite consistent with M06 frequency predictions (both shifts and actual frequency values) for the methyl-equatorial form of CH<sub>3</sub>SiCl<sub>3</sub>-NH<sub>3</sub>. Analogous matrix-IR experiments with CH<sub>3</sub>GeCl<sub>3</sub> and NH<sub>3</sub> yielded less conclusive results. Fewer product bands were observed overall, and a few peaks were only observed in annealing experiments. Nonetheless, two peaks were consistent with the methyl-equatorial form of CH<sub>3</sub>GeCl<sub>3</sub>-NH<sub>3</sub>, yet some product bands seem to agree with M06 predictions for the "long-bond", R-axial form of the complex. Finally, we presented pointwise (M06/aug-cc-pVTZ) maps of the M-N potential curves for both R-equatorial and R-axial forms of CH<sub>3</sub>SiCl<sub>3</sub>-NH<sub>3</sub> and CH<sub>3</sub>GeCl<sub>3</sub>-NH<sub>3</sub>. These curves are remarkably anharmonic and, in the case of the R-axial geometries, highlight the occurrence of two sets of equilibrium structures, the distinct minima along the M-N coordinate, and also convey the barriers between them. For the R-equatorial geometries of CH<sub>3</sub>SiCl<sub>3</sub>-NH<sub>3</sub> and CH<sub>3</sub>GeCl<sub>3</sub>-NH<sub>3</sub>, we also explored the effects of dielectric media on the M-N potential, using PCM/M06/aug-cc-pVTZ, with  $\varepsilon$  = 1.5 to 10. The curves at the upper end of this range of  $\varepsilon$ -values

indicate that the structures would change significantly in condensed-phased media in spite of the fact that the interaction evolves from an H-bond (C-H--N) to a tetrel bond (N $\rightarrow$ M) as the M-N coordinate is compressed. The inner regions of the potentials are flat and preferentially stabilized via interactions with the dielectric media, which causes the global minima to shift inward at higher  $\epsilon$ -values.

#### **ACKNOWLEDGMENT**

This work was made possible via CPU time allotted through the Blugold Supercomputing Cluster (BGSC) at UW - Eau Claire and via the MER-CURY Consortium.

#### **AUTHOR CONTRIBUTIONS**

James A. Phillips: Conceptualization; data curation; formal analysis; funding acquisition; investigation; supervision; validation; writing-original draft; writing-review and editing. Anna R. Ley: Data curation; formal analysis; investigation; validation; writing-original draft. Patrick W. Treacy: Data curation; formal analysis; investigation; validation; writing-original draft. Benjamin M. Wahl: Data curation; formal analysis; investigation. Brittany C. Zehner: Data curation; formal analysis; investigation; validation; writing-original draft. Benjamin M. Data curation; formal analysis; funding acuisition; investigation; methodology; validation; writing-review and editing. Samuel Gillespie: Data curation; formal analysis: investigation.

#### ORCID

James A. Phillips https://orcid.org/0000-0002-6697-7004 Kelling J. Donald https://orcid.org/0000-0001-9032-4225

#### REFERENCES

- [1] https://www.nobelprize.org/prizes/chemistry/1969/hassel/lecture/ (accessed: March 11, 2020).
- [2] H. A. Bent, Chem. Rev. 1968, 68, 587.
- [3] J. Rose, Molecular complexes, 1st ed., Pergamon Press, Oxford; New York 1967.
- [4] R. S. Mulliken, W. B. Person, Molecular complexes: A lecture and reprint volume, Wiley-Interscience, New York 1969.
- [5] J. Yarwood, Spectroscopy and structure of molecular complexes, Plenum Press, London; New York 1973.
- [6] R. Foster, Molecular complexes, Crane, Russak & Co., New York 1973.
- [7] V. Jonas, G. Frenking, M. T. Reetz, J. Am. Chem. Soc. 1994, 116, 8741.
- [8] G. Frenking, K. Wichmann, N. Frohlich, C. Loschen, M. Lein, J. Frunzke, V. M. Rayon, Coord. Chem. Rev. 2003, 238, 55.
- [9] G. R. Desiraju, P. S. Ho, L. Kloo, A. C. Legon, R. Marquardt, P. Metrangolo, P. Politzer, G. Resnati, K. Rissanen, Pure Appl. Chem. 2013, 85(8), 1711.
- [10] G. Cavallo, P. Metrangolo, R. Milani, T. Pilati, A. Priimagi, G. Resnati, G. Terraneo, Chem. Rev. 2016, 116, 2478.
- [11] S. J. Grabowski, Coord. Chem. Rev. 2020, 407, 213171.
- [12] A. Bauza, T. J. Mooibroek, A. Frontera, Ange. Chem. Int. Ed. 2013, 52, 12317.
- [13] J. Rezac, A. de la Lande, Phys. Chem. Chem. Phys. 2017, 19, 791.
- [14] K. R. Leopold, M. Canagaratna, J. A. Phillips, Acc. Chem. Res. 1997, 30, 57.
- [15] J. A. Phillips, Theor. Chem. Acc. 2016, 136, 16.
- [16] W. A. Burns, K. R. Leopold, J. Am. Chem. Soc. 1993, 115, 11622.
- [17] S. W. Reeve, W. A. Burns, F. J. Lovas, R. D. Suenram, K. R. Leopold, J. Phys. Chem. 1993, 97, 10630.
- [18] J. A. Phillips, J. A. Halfen, J. P. Wrass, C. C. Knutson, C. J. Cramer, Inorg. Chem. 2006, 45, 722.
- [19] A. A. Eigner, J. A. Rohde, C. C. Knutson, J. A. Phillips, J. Phys. Chem. B 2007, 111, 1402.
- [20] S. J. Grabowski, ChemPhysChem 2015, 16, 1470.
- [21] A. R. Buchberger, S. J. Danforth, K. M. Bloomgren, J. A. Rohde, E. L. Smith, C. C. A. Gardener, J. A. Phillips, J. Phys. Chem. B 2013, 117(39), 11687.
- [22] J. A. Phillips, C. J. Cramer, J. Phys. Chem. B 2007, 111, 1408.
- [23] H. M. Helminiak, R. R. Knauf, S. J. Danforth, J. A. Phillips, J. Phys. Chem. A 2014, 118, 4266.
- [24] A. W. Waller, N. M. Weiss, D. A. Decato, J. A. Phillips, J. Mol. Struct. 2017, 1130, 984.
- [25] N. J. Hora, B. M. Wahl, C. Soares, S. A. Lara, J. R. Lanska, J. A. Phillips, J. Mol. Struct. 2018, 1157, 679.
- [26] K. J. Donald, M. Tawfik, J. Phys. Chem. A 2013, 117, 14176.
- [27] K. J. Donald, E. Befekadu, S. Prasad, J. Phys. Chem. A 2017, 121, 8982.
- [28] P. Politzer, J. S. Murray, T. Clark, G. Resnati, Phys. Chem. Chem. Phys. 2017, 19, 32166.
- [29] T. Clark, M. Hennemann, J. S. Murray, P. Politzer, J. Mol. Model. 2007, 13, 291.
- [30] T. Brinck, A. N. Borrfors, J. Mol. Model. 2019, 25, 125.
- [31] M. J. Frisch, G. W. Trucks, H. B. Schlegel, G. E. Scuseria, M. A. Robb, J. R. Cheeseman, G. Scalmani, V. Barone, B. Mennucci, G. A. Petersson, H. Nakatsuji, M. Caricato, X. Li, H.P. Hratchian, A.F. Izmaylov, J. Bloino, G. Zheng, J. L. Sonnenberg, M. Hada, M. Ehara, K. Toyota, R. Fukuda, J. Hasegawa, M. Ishida, T. Nakajima, Y. Honda, O. Kitao, H. Nakai, T. Vreven, J. A. Montgomery, J. E. Peralta, Jr., F. Ogliaro, M. Bearpark, J. J. Heyd, E. Brothers, K. N. Kudin, V. N. Staroverov, T. Keith, R. Kobayashi, J. Normand, K. Raghavachari, A. Rendell, J. C. Burant, S. S. Iyengar, J. Tomasi, M. Cossi, N. Rega, J. M. Millam, M. Klene, J. E. Knox, J. B. Cross, V. Bakken, C. Adamo, J. Jaramillo, R. Gomperts, R. E. Stratmann, O. Yazyev, A. J. Austin, R. Cammi, C. Pomelli, J. W. Ochterski, R. L. Martin, K. Morokuma, V. G. Zakrzewski, G. A. Voth, P. Salvador, J. J. Dannenberg, S. Dapprich, A. D. Daniels, Ö. Farkas, J. B. Foresman, J. V. Ortiz, J. Cioslowski, D. J. Fox, Gaussian 09, Rev., C. 01, Wallingford CT, Gaussian, Inc., 2010.
- [32] D. J. Giesen, J. A. Phillips, J. Phys. Chem. A 2003, 107, 4009.
- [33] C. J. Cramer, Essentials of computational chemistry: Theories and models, 2nd ed., John Wiley and Sons, West Sussex, UK 2005.
- [34] Y. Zhao, D. G. Truhlar, Acc. Chem. Res. 2008, 41, 157.



- [35] J. D. Chai, M. Head-Gordon, Phys. Chem. Chem. Phys. 2008, 10, 6615.
- [36] F. Weinhold, C. R. Landis, Discovering chemistry with natural bond orbitals, Wiley, Hoboken, NJ 2012, p. xii.
- [37] A. E. Reed, R. B. Weinstock, F. Weinhold, J. Chem. Phys. 1985, 83, 735.
- [38] J. Tomasi, Theor. Chem. Acc. 2004, 112, 184.
- [39] J. P. Wrass, D. Sadowsky, K. M. Bloomgren, C. J. Cramer, J. A. Phillips, Phys. Chem. Chem. Phys. 2014, 16, 16480.
- [40] J. A. Phillips, S. J. Danforth, N. J. Hora, J. R. Lanska, A. W. Waller, J. Phys. Chem. A 2017, 121, 9252.

**How to cite this article**: Phillips JA, Ley AR, Treacy PW, et al. Structural and energetic properties of RMX<sub>3</sub>-NH<sub>3</sub> complexes. *Int J Quantum Chem.* 2020;120:e26383. https://doi.org/10.1002/qua.26383